R-2394

Available online at www.sciencedirect.com
ScienceDirect
ELSEVIER
J. Chem. Thermodynamics 39 (2007) 507–530
JCT
www.elsevier.com/locate/jct

Apparatus for wide-ranging, high-accuracy fluid (p, ρ, T) measurements based on a compact two-sinker densimeter ☆

Mark O. McLinden [a,*], Cornelia Lösch-Will [b]

[a] *Physical and Chemical Properties Division, National Institute of Standards and Technology, 325 Broadway, Mailstop 838.07, Boulder, CO 80305, USA*
[b] *Rubotherm Präzisionsmesstechnik, GmbH, Universitätsstraße 142, Bochum D-44799, Germany*

Received 31 May 2006; received in revised form 16 September 2006; accepted 20 September 2006
Available online 28 September 2006

Available online at www.sciencedirect.com
ScienceDirect
J. Chem. Thermodynamics 39 (2007) 507–530
JCT
www.elsevier.com/locate/jct

Apparatus for wide-ranging, high-accuracy fluid (p, ρ, T) measurements based on a compact two-sinker densimeter ☆

Mark O. McLinden [a,*], Cornelia Lösch-Will [b]

[a] *Physical and Chemical Properties Division, National Institute of Standards and Technology, 325 Broadway, Mailstop 838.07, Boulder, CO 80305, USA*
[b] *Rubotherm Präzisionsmesstechnik, GmbH, Universitätsstraße 142, Bochum D-44799, Germany*

Received 31 May 2006; received in revised form 16 September 2006; accepted 20 September 2006
Available online 28 September 2006

Abstract

An apparatus for high-accuracy fluid (p, ρ, T) measurements over wide ranges of temperature, pressure, and density (90 K to 520 K; 0 MPa to 40 MPa; 5 kg · m^{-3} to 1700 kg · m^{-3}) is described. The densimeter is based on the Archimedes (buoyancy) principle and is a two-sinker system incorporating a magnetic suspension coupling. The density is obtained directly, without the need for calibration fluids. The complete apparatus, including the thermostat, pressure and temperature measuring systems, auxiliary systems, and computer control, is described. The determination of the sinker volumes and calibrations of the measuring systems are detailed. The traceability to national standards and fundamental SI quantities is emphasized. The uncertainty ($k = 2$) in density is 0.0025% + 0.0006 kg · m^{-3} at 293 K and 0.1 MPa. The uncertainty increases to 0.015% + 0.001 kg · m^{-3} at the upper and lower temperature limits of the apparatus and a pressure of 40 MPa, primarily due to increased uncertainties in the sinker volumes. The uncertainty in temperature is 0.004 K and that in pressure ranges from 0.005% to 0.05%. Density measurements on high-purity nitrogen and helium demonstrate the performance of the densimeter and confirm the stated uncertainties. New data are presented for a high-density fluoroether; these measurements demonstrate the capabilities for liquids.

Keywords: Helium; Nitrogen; Pressure–density–temperature behavior; 2-Trifluoromethyl-3-ethoxydodecafluorohexane; Two-sinker densimeter

1. Introduction

The pressure–density–temperature ((p, ρ, T)) properties of fluids are key thermophysical property data needed for the development of accurate equations of state required to predict the efficiency of working fluids, to assure equity in the domestic and international trade of chemicals, fuels, and related fluids, and to enable accurate design and efficient control of chemical process equipment.

We describe a new instrument for wide-ranging fluid (p, ρ, T) measurements. The goals for the present instrument were, first, to achieve the lowest practical uncertainties compatible with the requirement of automated operation over a wide range of temperature and pressure, and, second, to develop an absolute instrument, *i.e.*, one independent of calibration fluids. The density is associated with a measured temperature and pressure to define a (p, ρ, T) state point, and, thus, the measurements of temperature and pressure must both be of the same high quality.

Applications of this instrument will include studies of fundamental fluid behavior to test and improve fluid property models, measurements of industrially important fluids requiring high-accuracy properties, and certification of standard reference materials for density, which would then be used in the calibration of industrial densimeters.

☆ Contribution of the National Institute of Standards and Technology. Not subject to copyright in the United States.

* Corresponding author. Tel.: +1 303 497 3580; fax: +1 303 497 5224.
E-mail addresses: markm@boulder.nist.gov (M.O. McLinden), cornelia.loesch-will@rubotherm.de (C. Lösch-Will).

0021-9614/$ - see front matter © 2006 Elsevier Ltd. All rights reserved.
doi:10.1016/j.jct.2006.09.012

2. Apparatus description

2.1. Principle of operation

The Archimedes principle dates to antiquity but remains among the simplest and most accurate techniques for the determination of density. It involves weighing a "sinker" of known volume V while it is suspended in the fluid of interest. The balance reading W is the difference between the sinker mass and the buoyancy of the fluid:

$$W = m - \rho V, \tag{1}$$

which is rearranged to yield the fluid density ρ:

$$\rho = \frac{m - W}{V}. \tag{2}$$

Calibration fluids are not required. The straightforward application of the Archimedes principle has yielded some of the most accurate fluid densities ever measured. For example, Masui *et al.* [1] have determined the density of water at near-ambient conditions with an uncertainty of less than 1 ppm (1 part per million) using the basic Archimedes technique.

However, the simple Archimedes experiment in which a sinker of known volume is suspended below a balance *via* a fine filament is limited to the narrow range of conditions tolerable by the balance. For wide-ranging measurements, another approach is needed, and the most successful has been the combination of the Archimedes principle with magnetic suspension. A magnetic suspension coupling transmits the weight of the sinkers to the balance, and separates the fluid, which may be at extremes of temperature and/or pressure, from the balance, which is at ambient conditions.

The accuracy of the Archimedes techniques can be improved by the use of two sinkers. In particular, the two-sinker technique developed by Kleinrahm and Wagner [2] has proven very successful, and this approach was chosen for the present instrument. For the two-sinker technique, the density is given by

$$\rho = \frac{(m_1 - W_1) - (m_2 - W_2)}{(V_1 - V_2)}, \tag{3}$$

where the subscripts refer to the two sinkers. The measurement of density, thus, requires the determination of the masses and volumes of the sinkers and the weighing of the sinkers (*via* the magnetic suspension coupling) while they are immersed in the fluid. Systematic errors, including surface adsorption, balance nonlinearity, and the influence of magnetic materials on the coupling are greatly reduced by the use of two sinkers with the same mass, same surface area, and same surface material, but very different volumes.

A photograph of the entire apparatus is shown in figure 1, and a simplified block diagram of the major systems is shown in figure 2. It consists of the following key components:

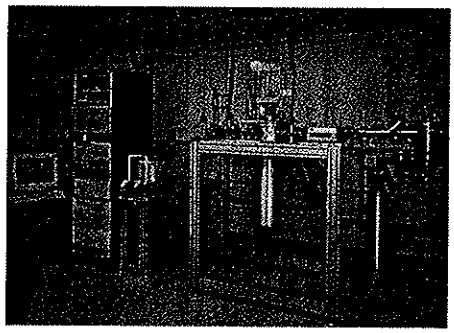

FIGURE 1. Photograph of the two-sinker densimeter. The key components are, from left to right, computer display; instrument rack; separate hydrostatic apparatus for sinker volume determinations; main part of densimeter with the balance in its draft hood at the top and the vacuum chamber containing the measuring cell at the bottom; and vacuum system. A mechanical vacuum pump, two circulating baths and a gas compressor are not visible.

- the two sinkers, which, together with a balance, the magnetic suspension coupling, and a mechanism to pick up each sinker constitute the density measuring system;
- the density measuring system, integrated with a measuring cell (pressure vessel) that contains the fluid of interest;
- a thermostat system incorporating fluid cooling and electrical heating;
- pressure- and temperature-measuring instruments;
- a computer, which controls the entire system and records the experimental data;
- auxiliary systems, such as a sample charging manifold and a vacuum system.

Each of these key components is now described in turn.

2.2. Density system and measuring cell

The density system, including the measuring cell (pressure vessel), sinkers, and magnetic suspension coupling, was manufactured by Rubotherm Präzisionsmesstechnik GmbH[1] and is described in detail by Lösch-Will [3]. The density system is depicted in figure 2, and is briefly described here.

One sinker is made of tantalum ($\rho = 16670\ \mathrm{kg \cdot m^{-3}}$) and the other of titanium ($\rho = 4507\ \mathrm{kg \cdot m^{-3}}$). Each has a nominal mass of 60 g to yield a volume difference of 9.74 $\mathrm{cm^3}$. The sinkers are contained within a measuring cell designed for pressures up to 40 MPa. The titanium sinker is in the shape of a right circular cylinder with a hole down its axis. The tantalum sinker is a thin-walled cylinder that has been "folded". The geometries are designed to yield equal surface areas; this feature, along with both sinkers being

[1] Certain trade names and products are identified only to adequately document the experimental equipment and procedure. This does not constitute a recommendation or endorsement of these products by the National Institute of Standards and Technology, nor does it imply that the products are necessarily the best available for the purpose.

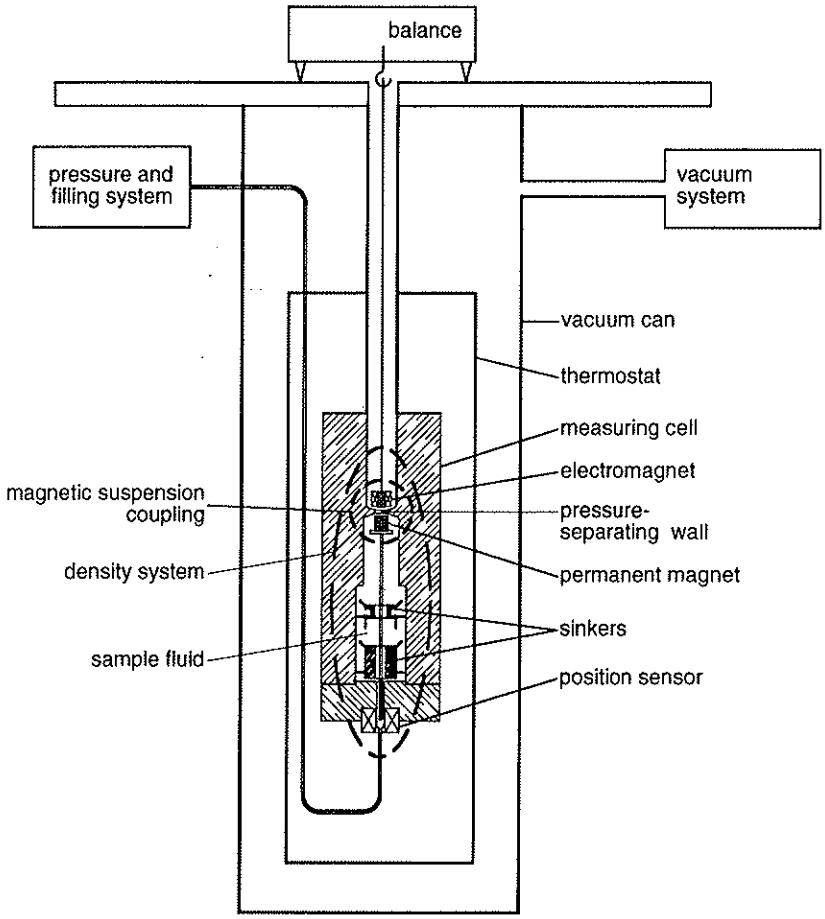

FIGURE 2. Block diagram of the densimeter and simplified schematic of the density system.

coated with gold, largely cancel any effects of surface adsorption.

Isolation of the fluid sample from the balance is accomplished with a magnetic suspension coupling. The central elements of the coupling are two magnets, one on each side of a nonmagnetic pressure-separating wall. The top magnet, which is an electromagnet with a ferrite core, is outside the pressure vessel and is suspended from the under-pan weighing hook of the balance. The bottom magnet, which is a permanent magnet, is inside the measuring cell, completely immersed in the fluid of interest, and is held in a freely suspended state by the electromagnet. A position sensor is also part of the coupling, and the stable suspension is maintained by means of a feedback control circuit making fine adjustments in the electromagnet current. The sinkers are picked up by a "lifting fork", connected to the permanent magnet. The lifting fork engages small pins on the sinkers, and through vertical and rotational motion it is able to pick up one sinker at a time. The weight of the sinkers is thus transmitted to the balance (Sartorius CC111). The magnetic suspension coupling/balance combination is stable and repeatable at the microgram level to yield a resolution in density of 0.0001 $kg \cdot m^{-3}$.

Compared to previous instruments, such as the one described by Kleinrahm and Wagner [2], the present instrument incorporates a number of improvements which are detailed by Lösch-Will [3]. These include a higher resolution in the density, a higher allowable operating pressure, a new mechanism for exchanging the sinkers, and a more compact arrangement. The compact geometry requires a smaller fluid charge and reduces temperature gradients. The capabilities of the new density-measuring system necessitate corresponding attention to detail in the temperature and pressure systems.

2.3. Thermostat and temperature system

2.3.1. Thermostat

The thermostat provides a uniform and controlled temperature environment for the fluid sample and magnetic suspension coupling. The thermostat is a vacuum-insulated cryostat-type design. A detailed diagram of the thermostat and density system is shown in figure 3. Multiple layers of active (heated or cooled) and passive shields are used. The innermost element, which includes the measuring cell and magnetic suspension coupling, is controlled within 2 mK of a constant temperature with an uncertainty in temperature of 4 mK.

The innermost level of the shielding, the "inner shield" is clamped to a "heating collar" at the top of the measuring

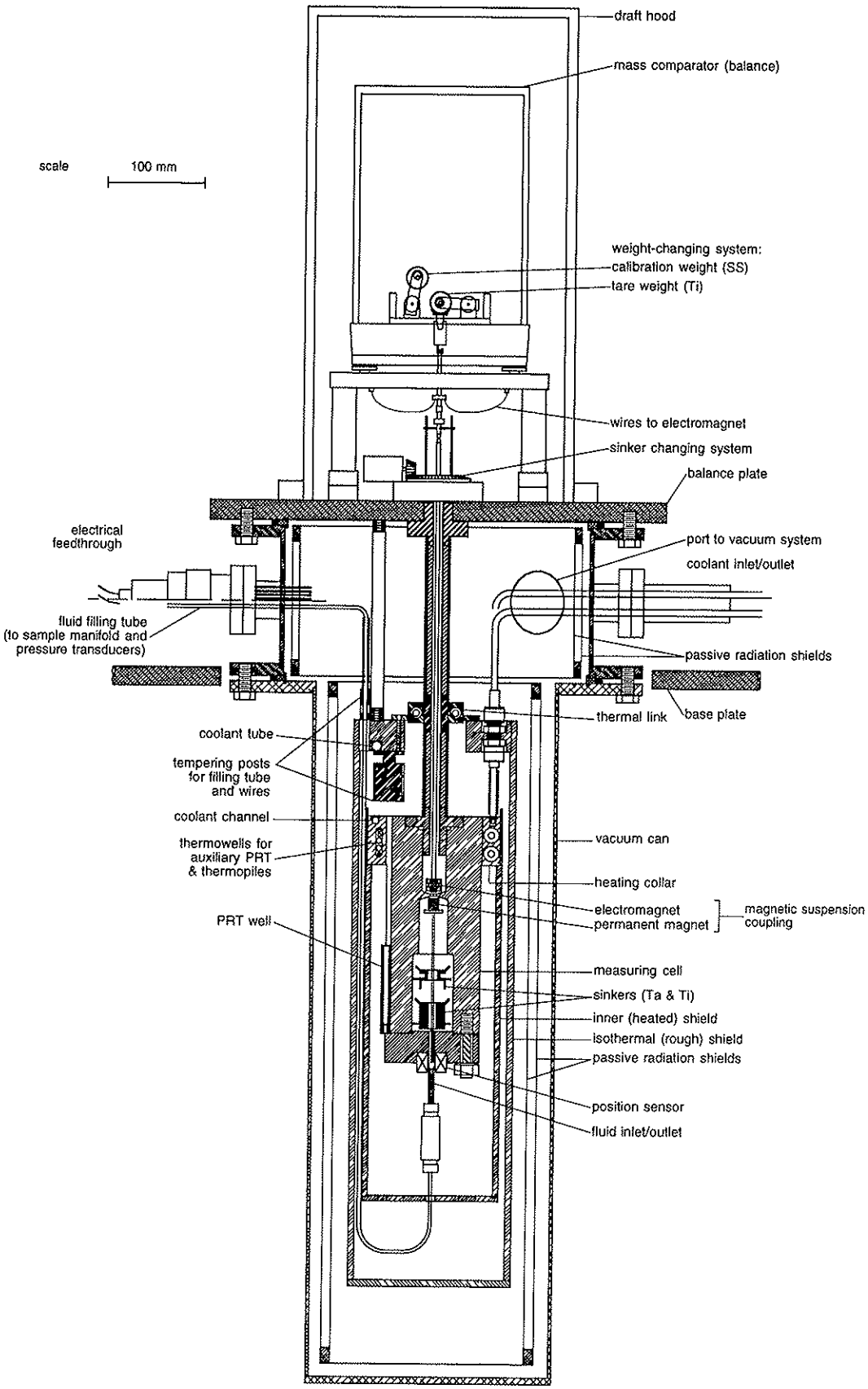

FIGURE 3. Detailed schematic of the density system and thermostat.

cell, but it is separated from the bottom portion of the cell. Nearly all the heat transfer to the surrounding "rough shield" (described below) is offset by heaters on the inner shield and heating collar. Thus the bottom portion of the cell containing the fluid sample is nearly adiabatic, resulting in very small temperature gradients in the fluid sample. Since there is good conduction heat transfer between the top of the cell and the inner shield, the difficulty of controlling a truly adiabatic cell is avoided.

The heating collar is clamped to the top of the measuring cell. The small (approximately 0.2 W) heat leak from the cell to the rough shield at steady-state conditions is offset by an electric heater fitted into a groove in the top of the heating collar and additional heaters along the length of the inner shield. To minimize the generation of magnetic fields, the heaters consist of lengths of fine resistance wire in a bifilar geometry. The heaters are supplied by regulated DC power supplies (Hewlett–Packard model 6624A) at relatively low current. A fluid cooling channel is machined into the top surface of the heating collar; this channel is capped by a ring of copper brazed into place. Fluid is circulated through this channel only for rapidly cooling the cell between tests; it is not used during measurements.

The next level of the thermostat, the rough shield, surrounds the measuring cell and inner shield and is maintained at a temperature 0.5 K to 1 K cooler than that of the measuring cell. The temperature is constant to within 20 mK. This shield is suspended from the base plate of the apparatus by three Inconel tubes. An electric heater is placed in a groove on the top surface, and four additional electric heaters are in vertical grooves on the side of the shield. A channel machined into the top of the shield accepts a length of copper tubing that serves as fluid heat exchanger. Liquid nitrogen or heat transfer fluid (either ethanol or a propylene glycol/water mixture) from an external circulating bath serves to cool the shield for measurements at temperatures below about 310 K. Cooling is not used at higher temperatures. The side and bottom of the isothermal shield consist of a simple "can" that is bolted to the top. There is no cooling of the side apart from conduction from the top. Heat transfer to the side is almost exclusively by radiation, which decreases at decreasing temperatures. Avoiding fluid connections on the shield side considerably simplifies assembly and disassembly.

The measuring cell/inner shield is suspended inside the rough shield by a "cell support". The mid-point of the cell support is thermally anchored to the rough shield. This shunts the majority of the heat flow to or from the balance plate, which is at ambient temperature, to the rough shield. The electrical leads, heat-transfer fluid lines, and the filling line to the measuring cell are also thermally anchored to the top of the rough shield.

The rough shield is surrounded by two passive radiation shields of thin aluminum foil. The outermost element of the thermostat is the vacuum can. The vacuum system consists of an oil diffusion pump plus liquid nitrogen cold trap backed by a mechanical vacuum pump. Feedthroughs for the electrical connections and fluid lines are made through a "feedthrough collar" located just above the top of the shields.

2.3.2. Materials of construction

Magnetic materials will affect the magnetic suspension coupling. The acceptable materials vary with the distance from the coupling. In the immediate vicinity of the magnets, only materials with a very low magnetic susceptibility can be used. For this reason, the measuring cell is constructed of a beryllium copper alloy. Within about 1 m of the coupling, ordinary copper, aluminum, and brass can be used, and small quantities of stainless steel are acceptable. At distances beyond about 1 m from the coupling, carbon steel and other ferromagnetic materials can be tolerated without disturbing the coupling. But it is important to keep strong permanent magnets at a distance of at least 2 m.

Care has been taken to construct the thermostat of nonmagnetic materials. The inner shield and rough shield are copper, and the vacuum chamber and base plate are aluminum. The balance plate (which forms the top of the vacuum chamber) is brass. The screws are mostly brass or silicon bronze. Two titanium bolts and fewer than 10 small screws of type 316 stainless steel are used, where high strength is required. The fluid fittings are type 316 stainless steel; these were tested before installation to verify that they were minimally magnetic. Tests of the sensitivity of the magnetic suspension coupling to magnetic materials show that these small quantities of very slightly magnetic stainless steel have no measurable effect on the measurements. The circulating bath and mechanical vacuum pump, which are made largely of steel and have large motors, are located at the corners of the laboratory, about 3 m from the apparatus. Steel gas cylinders are located at a similar distance.

2.3.3. Temperature system

Temperatures are measured with a variety of probes, depending on the required accuracy. The sample temperature requires the highest accuracy, and this temperature is measured by a 25 Ω capsule-type standard PRT (Rosemount model 162D) in a thermowell at the same level as the sinkers. This "cell SPRT", which measures the temperature reported in the (p, ρ, T) results, is measured with an AC resistance bridge (ASL model F700). The 25 Ω reference resistor for the bridge (Tinsley type 5685A) is thermostatted at 31.0 ± 0.2 °C in a small oil bath. The uncertainty of the cell PRT temperature is 4 mK, as detailed in section 3.5.

The heat to the measuring cell is controlled using the temperature of a second similar 25 Ω SPRT located in a thermowell in the heating collar at the top of the cell. This "control SPRT" is read by a nanovoltmeter (Keithley model 2002 with a model SCAN-2001 scanning card). This temperature has an uncertainty of 10 mK, but a short-term stability of 2 mK.

The temperatures of the top, side, and bottom of the rough shield are measured with type T (copper-constantan) thermopiles with their reference junctions located in thermowells adjacent to the control SPRT. These are measured with a second similar nanovoltmeter. These temperatures are used only for control of the heat to the shield. They have a short-term stability of 10 mK, however, the absolute temperature does not need to be known accurately. The temperatures of the room and the balance enclosure are measured with small 100 Ω PRTs read by the nanovoltmeter. The temperatures of the pressure transducers are measured with their internal quartz thermometers and internal circuitry.

The atmospheric pressure inside the draft hood is read by a pressure transducer (Paroscientific model 100A-01). The humidity inside the draft hood is read by a thin-film capacitance-type humidity transmitter (Vaisala model HMP237).

2.4. Filling and pressure measuring system

The pressure of the sample is measured with one of three vibrating-quartz-crystal-type pressure transducers with full-scale ranges of (1.38, 6.89, and 41.4) MPa (Paroscientific models 2200A, 9001K-001, and 9006K-001, respectively). For the helium measurements, the "high-range" transducer was replaced with a Paroscientific model 9000-10K-105 with a full-scale range of 68.9 MPa. They are in direct communication with the sample – the transducers are not oil-filled, and no differential pressure diaphragm is used. The transducers are housed in a close-fitting aluminum block thermostatted at 40.0 ± 0.1 °C by means of fluid channels connected to a circulating bath (Neslab model RTE140).

A valve manifold allows great flexibility in connecting the measuring cell to sample bottles, vacuum and the pressure transducers, and venting of the sample to the atmosphere or a recovery bottle. Figure 4 provides a schematic diagram. The measuring cell can be connected to a sample bottle either directly or thru an air-operated gas compressor (Superpressure, model 46-14025-2) capable of delivering pressures in excess of 40 MPa. A hand-operated, piston-type pressure generator (High Pressure Equipment, model 87-6-5) can be used to pressurize liquid samples. Valves to the vacuum system allow evacuation of the cell and/or each pressure transducer individually. Connections to both the mechanical roughing pump and high-vacuum diffusion pump plus liquid nitrogen cold trap are provided. The portion of the manifold connected to the measuring cell during density measurements is thermostatted to isolate the sample from fluctuations in room temperature.

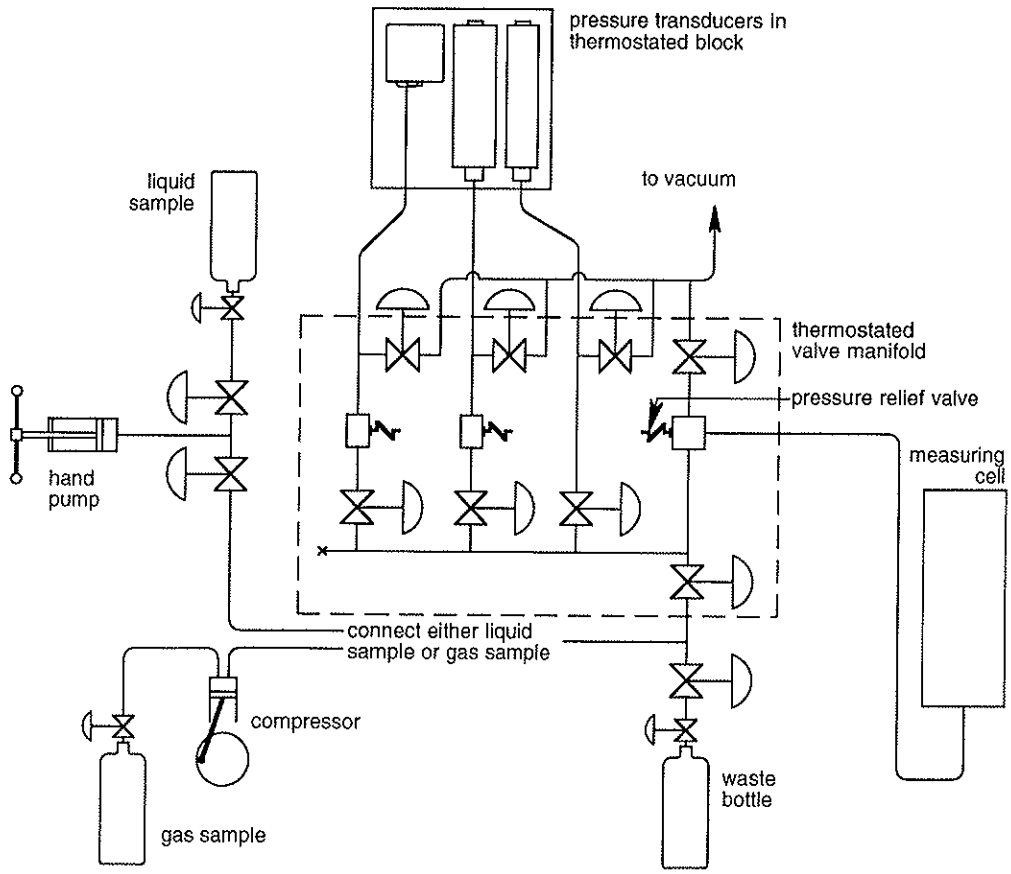

FIGURE 4. Schematic of the filling manifold and pressure system.

2.5. Control system and measurement sequence

Measurements are made along either isotherms starting at the highest pressure or pseudo-isochores starting at the lowest temperature. A computer program written in Pascal provides three main functions. The PC automates and controls the experiment, provides data logging of all the instrument readings, and serves as a PID controller for the electric heaters on the cell and shields.

All the instruments are scanned once each minute through either the serial RS-232 ports or an IEEE-488 interface. Temperatures are controlled by the modified PID algorithm of Hust *et al.* [4] implemented in the control program. A running average and standard deviation of the temperatures and pressures are computed for the preceding eight readings. When these are within preset tolerances of the set-point conditions, a weighing sequence is triggered. Weighings are made in the order: Ta sinker, Ti sinker, balance calibration weight, balance tare weight, balance tare weight (again), balance calibration weight, Ti sinker, and Ta sinker, for a total of eight weighings – two for each object. The weighing design is symmetrical with respect to time, and this will tend to cancel any drift in the temperature or pressure. The weighings are spaced 60 s to 90 s apart to give adequate time for the next object to be picked up and to allow the magnetic suspension coupling and balance to reach a stable weight.

The temperatures and pressures are recorded between each weighing and also before the first sinker weighing and after the final weighing. The resistances of the SPRTs, temperature and pressure periods of the pressure transducers, and individual balance readings are written to a file; more than 300 individual readings are recorded for each density determination. The calibrations for the various instruments are applied to the raw data, and the multiple readings are averaged in a separate analysis program.

Four to six replicate determinations of density are made at each (T,p) state point. The control program then automatically moves to the next temperature on an isochore or prompts the operator to vent the sample to the next pressure on an isotherm. Following every few isotherms or isochores, the cell is evacuated and the sinkers again weighed. In the measurements presented here, the calculated vacuum density differed slightly from zero (average value of $\pm 0.005\ \mathrm{kg \cdot m^{-3}}$), and this "apparatus zero" was subtracted from the measured densities.

2.6. Operating ranges

The results presented in section 4 demonstrate the densimeter over a wide range of temperature, pressure, and density. Although densities as low as $1.1\ \mathrm{kg \cdot m^{-3}}$ were measured for nitrogen, at such a low density the uncertainty is 0.057%. A practical lower limit would be about $5\ \mathrm{kg \cdot m^{-3}}$ where the uncertainty would be 0.015% to 0.024% depending on the temperature. In principle, the densimeter could be used at densities up to that of the titanium sinker ($4507\ \mathrm{kg \cdot m^{-3}}$). At very high fluid densities, however, the separation between the electromagnet and the permanent magnet is relatively large due to the low loading on the magnetic suspension coupling. This means that the titanium sinker would be barely lifted off its rest. Thus, the practical upper limit is near the maximum density of $1689\ \mathrm{kg \cdot m^{-3}}$ measured here.

The densimeter has been designed to operate at temperatures as low as 90 K when liquid nitrogen cooling is used, and limited tests using liquid nitrogen have been carried out. The present results, however, cover the more limited temperature range from 223 K to 500 K. The stated upper temperature limit of 520 K is based on the materials of construction.

3. Uncertainty determination

This instrument provides an absolute determination of the density, and it will be used to certify NIST Standard Reference Materials for density. This imposes the requirement of strict traceability to fundamental SI quantities. In this section we present a detailed discussion of calibration procedures and uncertainties.

3.1. Balance

The balance is a Sartorius CC111 mass comparator. All balances are affected by changes in ambient temperature and, more significantly, by changes in ambient air density. The balance is calibrated with a new system based on special calibration weights designed to cancel the effects of air buoyancy. A mechanism lowers tare and calibration weights onto a modified balance pan. The weights are cylindrical in shape and fabricated of titanium (tare weight) and stainless steel (calibration weight) so as to have different masses but nearly the same volume. This provides a balance calibration that is independent of air buoyancy – a significant advantage since low temperature tests are carried out with a dry nitrogen purge under the balance hood to avoid condensation of moisture onto the electromagnet, which is at the cell temperature. The standard mechanism of Rubotherm is used, but in a different way compared to its use with a single-sinker densimeter [5].

The calibration weight is 57.8 g, closely matching the balance loading when a sinker is weighed. The tare weight of 33.3 g brings the balance into its weighing range. The mass difference of 24.5 g covers nearly the full 31 g electronic weighing range of the balance. The different densities of the titanium and stainless steel allow the weights to be nearly identical in volume and surface area. Their volumes differ by 1.05%, as determined by a simple hydrostatic weighing in water.

The difference in mass of the calibration weights was determined *in situ* with the mass comparator. The mass comparator was first tared and calibrated with its built-in calibration function and a 20 g standard mass (Mettler, ASTM Class 1, with an uncertainty of 0.016 mg). Each

calibration weight was then weighed. The correction for air buoyancy on the standard mass was calculated using the BIPM air density equation [6] with ambient conditions measured with an electronic barometer (Vaisala model PTB220, uncertainty 0.01%), and a temperature and humidity transmitter (Vaisala model HMP237, uncertainty of 0.1 °C in temperature and 2% in relative humidity) with the sensor located next to the balance.

A balance calibration is carried out as an integral part of each density determination. A balance calibration factor is computed and applied to the weighings. Note that because of the buoyancy-free nature of the calibration weights, no further correction for air buoyancy is required in the calculation of sample density, since the sinkers are not in air.

The maximum drift in the balance calibration is less than 1 ppm/h, and it is usually less than 0.2 ppm/h. The uncertainty in the standard mass is less than 1 ppm. The uncertainty in the determination of the mass difference of the calibration weights is estimated to be 0.12 mg or 5 ppm of the 24.5 g difference. This effect is dominated by the uncertainty in the air buoyancy on the standard mass during the balance calibration. These effects contribute an uncertainty of 5 ppm to the density. The linearity of the balance as specified by the manufacturer is 3 μg, and the reproducibility was observed to be better than 2 μg. These contribute an uncertainty of 0.0004 $kg \cdot m^{-3}$ to the density.

3.2. Magnetic suspension coupling

The combination of the magnetic suspension coupling and mass comparator is stable and repeatable at the microgram level, and this yields a resolution in density of 0.0001 $kg \cdot m^{-3}$ [3]. The uncertainty in the density is thus dominated by potential systematic errors, such as uncertainty in the sinker volumes, drift in the balance, and the force transmission error in the magnetic suspension coupling.

The magnetic suspension coupling (MSC) transmits the buoyancy force on the sinkers to the balance, and any systematic error resulting from the influence of nearby magnetic materials could seriously affect the density measurement. This is known as a "force transmission error" [7]. The force transmission error arises from the interaction of the permanent magnet and electromagnet of the MSC with the pressure-separating wall and nearby magnetic materials, including the fluid being measured. The magnitude of this error is specific to each densimeter.

The automated calibration weights allow an analysis of the force transmission error. By weighing the sinkers in vacuum (using the MSC) and comparing this measurement to the known mass of the sinkers, the force transmission error for the apparatus is obtained:

$$\varepsilon_{\text{apparatus}} = \frac{W[\text{fork} + \text{sinker}] - \{W[\text{fork} + \text{cal wt}] + V_{\text{cal wt}}\rho_{\text{air}}\} - (m_{\text{sinker}} - m_{\text{cal wt}})}{m_{\text{sinker}}}, \quad (4)$$

where W refers to the balance reading for the weighing of the objects inside the bracket. The $V\rho$ term is needed to correct for air buoyancy on the calibration weight. Based on an analysis of 317 vacuum weighings carried out over the course of six months, the average error is 15.2 ppm with a standard deviation of 1.3 ppm. The effect of temperature over the range 250 K to 500 K is less than 2 ppm. The force transmission errors for the two sinkers are within 1 ppm of each other. The effect of moist air *versus* dry nitrogen under the balance hood is less than 2 ppm.

The magnetic properties of the test fluid itself lead to another source of systematic error in the MSC, as discussed by Wagner and Kleinrahm [8] and McLinden *et al.* [9]. This effect is related to the different amount of fluid between the permanent magnet and top of the measuring cell for the different weighings. The variation in the position of the permanent magnet is relatively large for a single-sinker densimeter – approximately 5 mm for the densimeter described by Wagner and Kleinrahm [8]. By contrast, for our two-sinker densimeter, the variation in the permanent magnet position between the two sinkers is only 0.3 mm for a fluid density of 1000 $kg \cdot m^{-3}$, and it decreases to nearly zero at low gas densities. McLinden *et al.* [9] demonstrate that the fluid-specific effect is proportional to the density and specific magnetic susceptibility of the fluid, and is on the order of a few tens of ppm for most fluids. It can be compensated with an uncertainty of 5 ppm.

3.3. Sinker volumes

3.3.1. Sinker volumes at 20 °C

The sinker volumes were determined using the hydrostatic comparator technique described by Bowman *et al.* [10,11]. This method differs from the traditional hydrostatic technique in that the known density is that of a solid object rather than a reference fluid, such as water. The standard and unknown objects are suspended in a fluid, but the fluid serves only to transfer the density knowledge of the standard to the unknown. The density of the fluid itself need not be known – it needs only to be constant over the time necessary to complete the measurement.

A separate apparatus was developed at NIST to carry out the sinker volume determinations. It is modeled closely after the apparatus of Bowman *et al.* [10]. A thermostatted fluid bath contains a "stage" that allows the submerged objects to be placed, one-at-a-time, onto a weighing "pan" that is suspended from the weighing hook of an analytical balance (Mettler AT201SE). The bath fluid is a high-density fluoroether (2-trifluoromethyl-3-ethoxydodecafluorohexane) manufactured by the 3M Company. This fluid has several advantages over water. Its high density of approximately 1631 $kg \cdot m^{-3}$ at 293 K, increases the buoyancy force on

the submerged objects and thus the sensitivity of the volume determination. Its low surface tension (16 N/m compared to 73 N/m for water) decreases the forces on the suspension wire. This and the much higher gas solubility compared to that of water greatly reduce the problems associated with small air bubbles clinging to the objects.

The standards are made of hyperpure, float-zone, single-crystal silicon. They are in the shape of right circular cylinders (49.8 mm diameter by 22.1 mm high) with a nominal mass of 100 g. Their densities were determined and certified by the NIST Mass Group [12] with an uncertainty ($k = 2$) of 14 ppm, using techniques very similar to those described here.

The hydrostatic apparatus accommodates four objects – two standards and two unknowns. This allows the simultaneous determination of the volumes of the tantalum and titanium sinkers and also provides the redundancy that permits a statistical analysis of the measurements. The experiment involves a series of A–B–A type weighings to yield ratios of the volumes of A and B. The experiment comprises 16 weighings:

A–B–A–C–A–D–A–D–B–D–C–D–C–B–C–B,

where "A" is standard #1, "B" is the tantalum sinker, "C" is standard #2, and "D" is the titanium sinker. This design yields the ratios AB, AC, AD, DA, DB, DC, CD, CB, and BC. The A–B–A design compensates for any linear drift in the balance zero and drift in the fluid density over the course of the experiment.

The volume ratios and resulting sinker volumes are given in table 1. The masses of the sinkers and standards were determined at least twice on different days, and the average value was used in the analysis. The measured volume ratios were determined at temperatures that differed slightly from the desired reference temperature of 293.15 K. A small (maximum 0.26 ppm) correction was applied by use of the literature values of the thermal expansion coefficient (Swenson [13] for silicon and Touloukian *et al.* [14] for tantalum and titanium) to adjust the volume ratios to the reference temperature. The experimental design provides a number of consistency checks. The redundant determinations of the volumes are very consistent, with a standard deviation of 0.85 ppm for the tantalum sinker and 1.7 ppm for the titanium sinker.

TABLE 1
Volume ratios and sinker masses m and volumes V determined by the hydrostatic comparator technique

Object	Ratio	Measured volume ratio	Ratio adjusted to 293.15 K	m/g	V/cm^3
Tantalum sinker	AB	11.746127	11.746129		3.610246
	CB	11.774715	11.774718		3.610248
	BC	0.084928	0.084928		3.610242
	Average			60.17796	3.610245
					$\sigma = 0.000003$
Titanium sinker	AD	3.177097	3.177098		13.347530
	DA	0.314753	0.314753		13.347530
	DC	0.313989	0.313989		13.347572
	CD	3.184823	3.184824		13.347566
	Average			60.16341	13.347549
					$\sigma = 0.000023$

The overall uncertainty in volume varies from 14 ppm to 29 ppm ($k = 2$), with objects having the highest density (*i.e.*, the smallest volume and buoyancy force) having the highest uncertainties. But the difference in the volumes of the two sinkers is the important quantity for the determination of density. Here, not all the errors are independent. For example, the uncertainty in the density of the silicon standards is a major component of the overall uncertainty, but an error in the silicon density will cause both sinker densities to be either high or low. Thus, there is a reduction in the uncertainties related to these errors, and the resulting total uncertainty in the volume difference is 24 ppm.

The experimental design also yields the volume ratios of the two standards and of the two sinkers; these allow a further check of consistency. The measured volume ratio of the silicon standards (AC) can be compared to the value calculated using the known values of mass and density. The directly measured ratio of the sinker volumes (DB) can be compared to the value obtained from the volumes calculated from the other ratios. These are compared in table 2 and are seen to be well within the estimated uncertainties.

3.3.2. Variation of sinker volumes with temperature and pressure

The sinker volumes determined at 20 °C must be adjusted for temperature and pressure. The linear thermal expansion of tantalum and titanium was measured over the range 100 K to 778 K by the Materials Research Institute of Ruhr Universität [15]. The samples used were taken from the same stock of Ta and Ti used to fabricate our sinkers. Titanium is anisotropic and its thermal expansion was measured both parallel and perpendicular to the axis of the raw bar stock. The volume expansion coefficient for titanium is taken to be twice the linear expansion across the diameter plus the expansion along the axis. Based on the technique, scatter in the data, and hysteresis observed between heating and cooling tests, the estimated uncertainty in the sinker volumes based on these thermal expansion data are $1.2 \cdot 10^{-6} \cdot (T/\mathrm{K} - 293.15)$, or 84 ppm at 223 K and 250 ppm at 500 K.

The calculated sinker volumes were further modified with an analysis of low-density gas data. The method is detailed elsewhere [16], but is briefly described here. Gas

TABLE 2
Volume ratios determined by hydrostatic weighing compared to calculated values

Ratio	Measured value	Calculated value	$10^6 \cdot$ Difference
AC	0.997576	0.997571	5.0
DB	3.697088	3.697131	11.6

densities are measured at several (nearly identical) pressures along two isotherms. The densities at corresponding pressures were ratioed and extrapolated to zero pressure, where the ideal-gas law applies:

$$\frac{\rho(T)}{\rho(T_{\mathrm{ref}})} = \frac{T_{\mathrm{ref}}}{T}, \tag{5}$$

where T_{ref} is the temperature of the hydrostatic sinker volume determination (293.15 K). The basic concept is that of a gas thermometer, except that density ratios at constant pressure are measured and extrapolated rather than the pressure ratios at constant density, as in a traditional constant-volume gas-thermometer. The difference between the extrapolated density ratio and the measured temperature ratio for a given pair of isotherms is interpreted as either the error in the indicated temperature relative to the thermodynamic temperature or the error in the sinker volumes. The temperatures are known to 4 mK (equivalent to 16 ppm at 250 K and 8 ppm at 500 K), so this technique was used to adjust the sinker volumes. The analysis used data on argon, neon, and nitrogen along 15 isotherms from 234 K to 505 K. The adjustment in the sinker volumes ranged from −45 ppm at 234 K to 0 ppm at 293 K to a maximum of 165 ppm at 438 K and decreasing to 84 ppm at 505 K. With this adjustment, the overall uncertainty in the sinker volume as a function of temperature is estimated to be $0.57 \cdot 10^{-6} \cdot (T/\mathrm{K} - 293.15)$, or 40 ppm at 223 K and 120 ppm at 505 K.

The pressure effects on the sinker volumes were calculated using the literature values for the bulk modulus [17]. At a pressure of 40 MPa this correction amounts to 204 ppm for the Ta sinker and 370 ppm for the Ti sinker. Taking a conservative estimate of a 10% uncertainty in the bulk modulus, this will contribute an uncertainty of 51 ppm to the density at 40 MPa.

3.4. Summary of uncertainty in density

The uncertainty in the density of a fluid is summarized in table 3. The ($k = 2$) uncertainty in density, including the effects of the balance, sinker volumes, and the magnetic suspension coupling can be expressed as:

$$u = 10^{-6} \cdot \left\{ [25^2 + 0.57 \cdot |T/\mathrm{K} - 293|]^2 + [1.25p/\mathrm{MPa}]^2 \right\}^{0.5} \times \rho_{\mathrm{fluid}}/(\mathrm{kg \cdot m^{-3}}) + (0.0006 + 1.8 \cdot 10^{-6}(T/\mathrm{K} - 293))/(\mathrm{kg \cdot m^{-3}}). \tag{6}$$

This is just the density uncertainty. The overall, or state point, uncertainty must also include uncertainties in the temperature and pressure and the effects of impurities in the sample, as described below.

3.5. Temperature system

The cell SPRT measures the temperature reported in the (p, ρ, T) data and requires the most accurate calibration.

TABLE 3
Summary of density uncertainties ($k = 2$) at various temperatures T

	T/K		
	250	293	500
Absolute errors (1 μg equivalent to 0.0001 kg · m^{-3} in density)			
Random scatter in weighings/μg	2	2	8
Balance linearity/μg	3	3	3
Drift in $\Delta m_{\mathrm{sinker}}$ (by vacuum weighing)/μg	5	5	5
Root sum of squares/(kg · m^{-3})	0.0006	0.0006	0.0010
Relative errors			
Sinker volumes at T_{ref}/10^{-6}	24	24	24
Sinker volumes as $f(T)$/10^{-6}; $p = 0.1$ MPa	25	0	118
Sinker volumes as $f(p)$/10^{-6}; $p = 40$ MPa	51	51	51
Force transmission error/10^{-6}	5	5	5
Balance calibration			
Uncertainty in standard mass/10^{-6}	1	1	1
Mass of tare & cal weights/10^{-6}	5	5	5
Root sum of squares at $p = 0.1$ MPa/10^{-6}	35	25	121
Root sum of squares at $p = 40$ MPa/10^{-6}	62	57	131

The control SPRT is used to control the temperature of the measuring cell; its uncertainty can be somewhat larger. The accuracy requirements for the other temperature sensors are an order of magnitude less stringent.

The control SPRT and cell SPRT are calibrated on ITS-90 using fixed-point cells. The R_0 for each PRT is established with a traditional water triple-point cell constructed of borosilicate glass and maintained in a distilled water/ice bath in a vacuum dewar (triple-point cells manufactured by Allen Scientific Glass and Pond Engineering were used at different times). The argon triple point (83.8058 K) is realized with a self-contained system (Pond Engineering, model K38). It consists of a metal cell containing 99.9999% pure argon with a central thermowell for the thermometer. The mercury triple point (234.3156 K) is realized with a metal cell containing 99.999999% pure mercury (Pond Engineering, model K18C). The indium and tin points (429.7485 K and 505.078 K, respectively, on ITS-90) are realized using fixed-point cells manufactured by Hart Scientific (models 5944 and 5945) and maintained in their model 9260 furnace. The Hart cells are metal-cased and use 99.9999% pure metals. The uncertainty ($k = 2$) assigned by the manufacturers is 2 mK or less for each system. Hydrostatic head and pressure corrections are applied to all the fixed points.

We confirmed the performance of the fixed point cells and our calibration procedures by checking the calibration of a SPRT calibrated by the NIST Thermometry Group. All five fixed points were within 2 mK of the NIST calibration. To date, two calibrations separated by eight months have been carried out for the cell PRT. The maximum change observed between calibrations was 0.6 mK.

The PRTs are calibrated as a system, meaning that the PRTs are merely removed from their thermowells in the

densimeter and inserted into the fixed point cells. The same instruments (voltmeter or resistance bridge), standard resistor, cables, and feedthroughs used in the density measurements are used in the calibration. We estimate the total ($k = 2$) uncertainty for the cell PRT, including the uncertainty in the fixed-point cells, nonlinearity in the resistance bridge, and drift in the PRT and standard resistor between calibrations, to be 4 mK.

The thermopiles measuring the temperature difference between the cell and the shield use standard thermocouple potentials [18]. These thermopiles were checked with the reference junction in a distilled water/ice bath and the measuring junction in a gallium melting point cell (YSI model 17402) and were found to be within 0.4% of the standard values. These are used only to control the shield temperature and are not critical measurements.

3.6. Pressure system

The pressure transducers are calibrated with piston gages. A gas-operated system (DH Instruments model PG7601) is used for the low- and medium-range transducers. Two different piston-cylinder sets are used. The set with a constant of 50 kPa · kg^{-1} is used for the low-range transducer; its total uncertainty ($k = 2$) in pressure is 14 ppm according to the manufacturer's NIST-traceable calibration. The medium-range transducer (as well as the lower portion of the high-range transducer) is calibrated with a piston-cylinder with $k_n = 200$ kPa · kg^{-1}; its uncertainty in pressure is 20 ppm. The high-range transducer is calibrated with a hybrid gas/oil system (DH model 5502) with a total uncertainty of 50 ppm.

The transducers are calibrated *in situ* by connecting the piston gage to the sample port of the filling manifold. This avoids any shock associated with transporting the transducers and the possibility of introducing leaks by disconnecting fittings. It also allows the transducers to be used and calibrated under identical thermostatting conditions. Although these transducers are temperature compensated, we have found that maintaining them at a constant temperature improves their performance beyond the manufacturer's specification of 0.01% full scale uncertainty. The major drift in the calibration over time is in the zero (vacuum) reading. The zero readings are regularly checked by opening the transducers to vacuum. This check is carried out every one to three weeks, and the pressure readings are adjusted by any drift.

The quartz temperature sensors in the transducers are based on the calibration provided by the manufacturer. The pressure function requires the temperature, but uncertainties in these temperatures are folded into the pressure calibration by virtue of using and calibrating the transducers at the same temperature.

The pressure transducers are located 38 cm above the mid-point of the sinkers in the measuring cell. The hydrostatic head associated with this height difference is calculated by a step-wise integration starting at the transducer and proceeding down the sample line to the cell. Temperatures are measured at three points along this path and interpolated at intermediate points. The local densities required in the calculation are computed with an equation of state. This head correction amounts to 20 ppm to 40 ppm of the total pressure for nitrogen and is less than 6 kPa for the high-density, compressed liquid measured here. The hydrostatic head correction contributes an uncertainty of, at most, 10 ppm to the pressure measurement.

Based on the uncertainties for the piston gages, the repeatability observed for these transducers, and the uncertainties associated with the hydrostatic head correction, we estimate the total ($k = 2$) uncertainty in pressure to be $\pm(0.0017\% + 0.06$ kPa) for $p < 1.3$ MPa; $\pm(0.0022\% + 0.34$ kPa) for $p < 6.8$ MPa, and $\pm(0.0051\% + 2.0$ kPa) for $p < 40$ MPa.

For some of the tests with nitrogen (described in section 4), the pressure in the cell was both generated and determined by the PG7601 piston gage. For these tests, the uncertainty in pressure was 0.0017% for $p < 1.3$ MPa and 0.0022% for $p \leqslant 7$ MPa.

4. First experimental results

4.1. Nitrogen

Measurements on nitrogen are presented. Nitrogen has perhaps the best-characterized density for any fluid apart from water, and is available in high purity. These characteristics make it an ideal fluid to demonstrate the capabilities of the densimeter.

4.1.1. Sample

The sample used was "VLSI-grade" nitrogen (Scott Specialty Gases). The specification for this gas is 99.9995% purity, and a cylinder analysis by the supplier indicated concentrations of oxygen, carbon dioxide, carbon monoxide, water, and total hydrocarbons of 0.2 ppm to 0.5 ppm. The concentration of hydrogen was 1 ppm for an overall purity of 99.9997%. Our own analysis by gas chromatography was consistent with the supplier's analysis. We also checked for the presence of argon and found none at a detection level of 1 ppm.

Based on the purity analysis, the molar mass of our sample was 28.01345 g · mol^{-1} or 1.0 ppm lower than the nominal value [19]. Any variation of the relative abundances of the ^{14}N and ^{15}N isotopes from the normal is unknown. We measure and report mass densities, but equations of state and virial coefficients are usually reported on a molar basis, and any use of our data in such analyses would be affected by sample purity at the 1 ppm level.

4.1.2. Experimental results

Nitrogen was measured at 103 (p, T) state points from 265 K to 500 K with pressures to 34 MPa. Four or more replicates were measured at each state point for a total of

TABLE 4
Experimentally measured pressures p and densities ρ_{exp} at temperatures T for nitrogen with a comparison to the densities calculated with the equation of state of Span *et al.* [20] ρ_{EOS}

T/K	p/MPa	ρ_{exp}/(kg · m^{-3})	$10^2(\rho_{exp} - \rho_{EOS})/\rho_{EOS}$
319.995	4.7758	50.1489	−0.0071
319.995	4.7758	50.1482	−0.0077
319.996	4.7758	50.1481	−0.0080
319.996	4.7759	50.1492	−0.0069
319.996	4.7759	50.1493	−0.0072
319.996	4.7759	50.1490	−0.0079
339.993	5.0821	49.9616	−0.0046
339.994	5.0820	49.9602	−0.0053
339.995	5.0820	49.9600	−0.0059
339.994	5.0820	49.9596	−0.0058
339.993	5.0819	49.9596	−0.0051
359.992	5.3853	49.7747	−0.0031
359.994	5.3855	49.7747	−0.0047
359.994	5.3855	49.7744	−0.0048
359.993	5.3854	49.7738	−0.0048
359.993	5.3854	49.7746	−0.0042
359.994	5.3855	49.7747	−0.0053
379.991	5.6858	49.5890	−0.0033
379.992	5.6857	49.5891	−0.0024
379.993	5.6858	49.5891	−0.0024
379.993	5.6857	49.5887	−0.0029
379.993	5.6857	49.5886	−0.0029
379.994	5.6857	49.5883	−0.0029
399.993	5.9838	49.4092	−0.0011
399.992	5.9838	49.4087	−0.0017
399.993	5.9837	49.4089	−0.0007
399.994	5.9837	49.4079	−0.0016
399.993	5.9836	49.4075	−0.0018
399.992	5.9836	49.4072	−0.0018
419.992	6.2786	49.2271	0.0004
419.993	6.2786	49.2276	0.0022
419.993	6.2786	49.2274	0.0020
419.991	6.2786	49.2274	0.0018
419.992	6.2786	49.2273	0.0014
439.992	6.5711	49.0504	0.0056
439.993	6.5711	49.0497	0.0046
439.994	6.5711	49.0500	0.0058
439.993	6.5710	49.0492	0.0049
459.994	6.8613	48.8758	0.0094
459.995	6.8613	48.8757	0.0094
459.996	6.8613	48.8759	0.0100
459.995	6.8614	48.8764	0.0093
459.994	6.8613	48.8757	0.0095
479.993	7.1487	48.7027	0.0148
479.994	7.1486	48.7024	0.0155
479.995	7.1487	48.7027	0.0161
479.996	7.1486	48.7016	0.0147
479.996	7.1486	48.7015	0.0148
499.996	7.4337	48.5313	0.0225
499.995	7.4337	48.5307	0.0207
499.995	7.4338	48.5310	0.0199
499.996	7.4338	48.5323	0.0230
499.997	7.4338	48.5317	0.0216
499.997	7.4339	48.5314	0.0207
319.996	10.1346	104.9993	0.0025
319.997	10.1349	105.0014	0.0024
319.998	10.1350	105.0021	0.0023
319.997	10.1349	105.0014	0.0020
319.997	10.1349	105.0019	0.0026
319.998	10.1350	105.0014	0.0018
339.996	10.8405	104.5890	0.0065
339.997	10.8405	104.5892	0.0070
339.997	10.8404	104.5886	0.0070
339.996	10.8404	104.5878	0.0065
339.996	10.8404	104.5878	0.0062
339.997	10.8404	104.5876	0.0065
359.994	11.5386	104.1820	0.0030
359.996	11.5386	104.1816	0.0034
359.996	11.5386	104.1809	0.0030
359.996	11.5385	104.1806	0.0029
359.995	11.5385	104.1806	0.0030
359.997	11.5385	104.1802	0.0033
379.994	12.2285	103.7783	0.0006
379.994	12.2284	103.7759	−0.0008
379.994	12.2283	103.7761	−0.0004
379.996	12.2284	103.7761	0.0002
379.996	12.2283	103.7749	−0.0004
379.995	12.2283	103.7752	−0.0004
399.995	12.9115	103.3879	0.0007
399.994	12.9115	103.3867	−0.0006
399.995	12.9112	103.3850	0.0006
399.994	12.9111	103.3833	−0.0008
399.996	12.9110	103.3836	0.0001
399.996	12.9110	103.3827	−0.0004
419.994	13.5869	103.0021	0.0028
419.994	13.5867	103.0011	0.0030
419.996	13.5868	103.0014	0.0030
419.997	13.5869	103.0019	0.0030
419.996	13.5867	102.9999	0.0021
419.996	13.5867	103.0010	0.0032
439.998	14.2554	102.6240	0.0073
439.997	14.2553	102.6222	0.0061
439.996	14.2551	102.6214	0.0065
439.998	14.2553	102.6225	0.0069
439.999	14.2552	102.6219	0.0072
439.997	14.2552	102.6215	0.0066
459.997	14.9175	102.2532	0.0116
459.996	14.9174	102.2530	0.0118
459.998	14.9173	102.2519	0.0114
459.997	14.9172	102.2509	0.0109
459.997	14.9172	102.2515	0.0115
459.997	14.9171	102.2504	0.0113
479.997	15.5726	101.8860	0.0175
479.996	15.5725	101.8857	0.0172
479.997	15.5724	101.8846	0.0170
479.998	15.5723	101.8835	0.0168
479.998	15.5723	101.8840	0.0173
479.997	15.5722	101.8829	0.0167
499.996	16.2208	101.5207	0.0235
499.996	16.2206	101.5190	0.0230
499.998	16.2205	101.5188	0.0238
499.998	16.2204	101.5181	0.0233
499.997	16.2204	101.5177	0.0228
499.996	16.2203	101.5167	0.0226
319.998	20.2098	198.7991	0.0005
319.999	20.2099	198.8005	0.0011
319.999	20.2097	198.7988	0.0008
319.998	20.2096	198.7985	0.0008
319.999	20.2095	198.7966	0.0006
319.999	20.2095	198.7961	0.0004
339.994	21.7843	198.0140	−0.0009
339.998	21.7841	198.0096	−0.0014
339.998	21.7841	198.0087	−0.0014
339.997	21.7838	198.0078	−0.0013
339.998	21.7838	198.0060	−0.0019

TABLE 4 (*continued*)

T/K	p/MPa	ρ_{exp}/(kg · m^{-3})	$10^2(\rho_{exp} - \rho_{EOS})/\rho_{EOS}$
339.999	21.7838	198.0068	−0.0012
359.994	23.3369	197.2465	−0.0010
359.996	23.3366	197.2431	−0.0013
359.997	23.3366	197.2426	−0.0012
359.998	23.3364	197.2410	−0.0010
359.998	23.3362	197.2387	−0.0014
359.998	23.3361	197.2376	−0.0017
379.996	24.8691	196.4970	−0.0014
379.998	24.8691	196.4959	−0.0015
379.999	24.8686	196.4924	−0.0015
379.998	24.8684	196.4927	−0.0010
379.997	24.8682	196.4920	−0.0009
379.999	24.8682	196.4910	−0.0009
399.998	26.3826	195.7740	−0.0002
399.997	26.3818	195.7697	−0.0001
399.999	26.3819	195.7696	0.0001
399.999	26.3813	195.7658	0.0000
399.997	26.3810	195.7629	−0.0008
399.999	26.3809	195.7628	−0.0001
419.996	27.8780	195.0695	0.0005
419.997	27.8769	195.0639	0.0012
419.997	27.8767	195.0645	0.0021
419.999	27.8765	195.0605	0.0011
419.998	27.8759	195.0582	0.0013
419.997	27.8757	195.0566	0.0011
439.999	29.3493	194.3481	0.0043
439.999	29.3489	194.3467	0.0045
439.999	29.3487	194.3454	0.0044
439.999	29.3483	194.3438	0.0049
439.999	29.3480	194.3416	0.0046
439.999	29.3477	194.3402	0.0047
459.999	30.8121	193.6903	0.0081
459.999	30.8107	193.6832	0.0080
460.000	30.8105	193.6813	0.0078
460.001	30.8101	193.6784	0.0079
460.001	30.8096	193.6773	0.0084
459.999	30.8092	193.6750	0.0079
480.000	32.2564	193.0345	0.0129
480.000	32.2560	193.0317	0.0125
480.001	32.2557	193.0316	0.0133
480.002	32.2553	193.0292	0.0132
480.001	32.2548	193.0268	0.0131
480.000	32.2545	193.0251	0.0129
499.998	33.6855	192.3964	0.0187
499.998	33.6836	192.3886	0.0192
500.000	33.6829	192.3842	0.0190
500.001	33.6825	192.3822	0.0191
499.998	33.6818	192.3795	0.0190
499.998	33.6812	192.3769	0.0190

Measurements along pseudo-isochores with pressures measured with the pressure transducer.

548 (p, ρ, T) data. Table 4 presents data measured along pseudo-isochores, and table 5 presents measurements along isotherms. The experimental temperature and pressure listed in the tables are the averages of the readings taken over the 12 min needed to complete a full density determination. The final column gives the difference of the measured densities with the equation of state of Span *et al.* [20] taking the temperature and pressure as the independent variables.

For some of the nitrogen measurements, the pressures were generated and measured with a piston gage (DH

TABLE 5

Experimentally measured pressures p and densities ρ_{exp} at temperatures T for nitrogen with a comparison to the densities calculated with the equation of state of Span *et al.* [20] ρ_{EOS}

T/K	p/MPa	ρ_{exp}/(kg · m^{-3})	$10^2(\rho_{exp} - \rho_{EOS})/\rho_{EOS}$
250.001	31.9163	377.5160	−0.0061
250.000	31.9156	377.5128	−0.0058
250.001	31.9150	377.5055	−0.0061
250.002	31.9148	377.5038	−0.0057
250.002	31.9143	377.4996	−0.0061
250.001	31.9138	377.4977	−0.0058
250.001	27.9228	345.6288	−0.0018
250.002	27.9228	345.6271	−0.0021
250.001	27.9223	345.6238	−0.0021
250.003	27.9224	345.6208	−0.0021
250.001	27.9219	345.6199	−0.0019
250.001	27.9217	345.6187	−0.0018
250.002	23.9208	309.0618	0.0028
250.003	23.9204	309.0561	0.0025
250.001	23.9186	309.0428	0.0031
250.003	23.9185	309.0379	0.0028
250.002	23.9182	309.0349	0.0026
250.001	23.9177	309.0332	0.0028
250.002	19.6724	264.4384	0.0045
250.002	19.6723	264.4371	0.0045
250.000	19.6721	264.4362	0.0041
250.001	19.6721	264.4357	0.0040
250.003	19.6720	264.4339	0.0045
250.002	15.9453	220.0776	0.0024
250.003	15.9456	220.0791	0.0026
250.001	15.9454	220.0780	0.0024
250.002	15.9453	220.0778	0.0026
250.003	15.9453	220.0762	0.0024
250.000	11.9443	167.5304	0.0021
250.002	11.9443	167.5306	0.0027
250.002	11.9443	167.5298	0.0025
250.001	11.9443	167.5305	0.0025
250.001	11.9443	167.5310	0.0022
250.002	11.9443	167.5299	0.0028
250.001	7.9220	111.2011	0.0002
250.003	7.9221	111.2012	0.0001
250.002	7.9221	111.2012	−0.0004
250.001	7.9220	111.2009	−0.0002
249.999	4.0320	55.8105	−0.0123
250.001	4.0320	55.8112	−0.0116
250.000	4.0320	55.8107	−0.0120
250.000	4.0320	55.8109	−0.0129
250.001	4.0320	55.8104	−0.0117
273.161	33.9662	356.4129	−0.0019
273.160	33.9654	356.4068	−0.0024
273.158	33.9644	356.4025	−0.0024
273.159	33.9637	356.3973	−0.0022
273.160	33.9631	356.3909	−0.0023
273.158	28.7937	318.0674	0.0012
273.160	28.7937	318.0651	0.0013
273.161	28.7933	318.0575	0.0003
273.160	28.7929	318.0570	0.0007
273.159	28.7924	318.0555	0.0010
273.159	24.5260	281.9219	0.0014
273.161	24.5260	281.9206	0.0017
273.161	24.5254	281.9148	0.0019
273.161	24.5250	281.9126	0.0019
273.159	24.5245	281.9097	0.0017
273.158	20.3090	241.7456	0.0037
273.159	20.3089	241.7448	0.0039

(*continued on next page*)

TABLE 5 (*continued*)

T/K	p/MPa	ρ_{exp}/(kg · m^{-3})	$10^2(\rho_{exp} - \rho_{EOS})/\rho_{EOS}$
273.161	20.3090	241.7430	0.0042
273.159	20.3085	241.7389	0.0037
273.158	20.3082	241.7355	0.0029
273.159	16.3763	200.1327	0.0014
273.158	16.3761	200.1314	0.0014
273.160	16.3760	200.1292	0.0016
273.160	16.3759	200.1274	0.0011
273.158	16.3759	200.1297	0.0013
273.159	12.1680	151.5676	0.0007
273.159	12.1681	151.5680	0.0005
273.158	12.1680	151.5667	−0.0004
273.158	12.1679	151.5658	−0.0002
273.160	12.1678	151.5632	−0.0005
273.160	8.1652	102.4802	0.0010
273.159	8.1652	102.4804	0.0010
273.160	8.1652	102.4790	0.0002
273.160	8.1651	102.4795	0.0013
273.158	8.1651	102.4783	−0.0001
273.158	8.1651	102.4798	0.0005
273.158	6.1725	77.4438	−0.0023
273.160	6.1726	77.4442	−0.0024
273.159	6.1726	77.4441	−0.0026
273.157	6.1725	77.4431	−0.0029
273.158	6.1725	77.4433	−0.0027
273.158	3.9692	49.6242	−0.0110
273.160	3.9692	49.6244	−0.0111
273.160	3.9692	49.6239	−0.0118
273.158	3.9692	49.6241	−0.0117
273.160	3.9693	49.6242	−0.0123
293.150	32.1475	317.9256	0.0002
293.150	32.1470	317.9221	0.0005
293.153	32.1466	317.9172	0.0007
293.151	32.1459	317.9116	−0.0001
293.151	32.1453	317.9093	0.0002
293.152	32.1451	317.9053	0.0000
293.152	32.1445	317.9018	0.0002
293.151	28.4130	290.4550	0.0015
293.154	28.4129	290.4526	0.0017
293.153	28.4119	290.4433	0.0008
293.151	28.4121	290.4478	0.0011
293.153	28.4122	290.4472	0.0015
293.154	28.4119	290.4438	0.0012
293.154	24.1765	256.0548	0.0017
293.152	24.1760	256.0518	0.0014
293.152	24.1758	256.0494	0.0014
293.154	24.1756	256.0474	0.0020
293.153	24.1752	256.0423	0.0011
293.151	19.5677	214.4565	0.0014
293.151	19.5677	214.4565	0.0016
293.153	19.5676	214.4572	0.0029
293.153	19.5674	214.4535	0.0021
293.152	19.5674	214.4528	0.0016
293.151	19.5671	214.4519	0.0023
293.151	15.9547	178.7821	−0.0001
293.152	15.9548	178.7837	0.0005
293.154	15.9549	178.7828	0.0000
293.153	15.9548	178.7829	0.0006
293.152	15.9546	178.7811	0.0000
293.154	15.9547	178.7812	0.0003
293.153	15.9547	178.7803	0.0001
293.152	15.9545	178.7796	−0.0003
293.152	11.9801	136.7194	0.0018
293.154	11.9801	136.7181	0.0012
293.152	11.9798	136.7158	0.0009

TABLE 5 (*continued*)

T/K	p/MPa	ρ_{exp}/(kg · m^{-3})	$10^2(\rho_{exp} - \rho_{EOS})/\rho_{EOS}$
293.151	11.9797	136.7149	0.0009
293.153	11.9797	136.7146	0.0017
293.153	11.9798	136.7158	0.0014
293.151	11.9796	136.7132	0.0008
293.151	7.9488	91.6890	0.0024
293.152	7.9488	91.6881	0.0020
293.151	7.9486	91.6871	0.0024
293.152	7.9486	91.6868	0.0016
293.152	7.9486	91.6869	0.0020
293.150	7.9486	91.6867	0.0015
293.151	5.9649	68.9510	0.0004
293.153	5.9649	68.9512	0.0014
293.152	5.9649	68.9516	0.0006
293.150	5.9649	68.9510	0.0000
293.153	5.9649	68.9517	0.0012
293.151	4.0048	46.2932	−0.0088
293.153	4.0048	46.2933	−0.0079
293.153	4.0048	46.2931	−0.0092
293.151	4.0048	46.2934	−0.0088
293.153	4.0048	46.2933	−0.0083
293.154	4.0048	46.2935	−0.0085
293.152	4.0048	46.2936	−0.0093
293.152	4.0049	46.2937	−0.0091
340.007	33.7203	281.3894	−0.0013
340.008	33.7195	281.3858	−0.0007
340.009	33.7193	281.3836	−0.0007
340.009	33.7187	281.3800	−0.0008
340.008	33.7185	281.3791	−0.0007
340.007	28.6080	247.9986	−0.0012
340.007	28.6078	247.9960	−0.0016
340.009	28.6076	247.9933	−0.0015
340.009	28.6072	247.9904	−0.0016
340.008	28.6068	247.9890	−0.0017
340.007	24.0699	215.4674	−0.0012
340.009	24.0698	215.4662	−0.0007
340.009	24.0697	215.4654	−0.0008
340.007	24.0692	215.4629	−0.0010
340.008	24.0693	215.4629	−0.0007
340.008	20.0727	184.4528	0.0006
340.007	20.0724	184.4501	0.0002
340.008	20.0722	184.4486	0.0004
340.010	20.0722	184.4470	0.0001
340.007	20.0719	184.4451	−0.0003
340.007	20.0717	184.4431	−0.0004
340.008	15.9615	150.2420	0.0004
340.007	15.9614	150.2409	0.0000
340.008	15.9615	150.2396	−0.0008
340.009	15.9613	150.2393	−0.0001
340.008	15.9612	150.2383	−0.0003
340.006	11.9619	114.8453	0.0015
340.007	11.9618	114.8449	0.0021
340.009	11.9618	114.8443	0.0020
340.008	11.9617	114.8441	0.0023
340.008	11.9617	114.8423	0.0011
340.010	7.7897	75.9998	0.0032
340.007	7.7897	76.0005	0.0036
340.008	7.7897	76.0006	0.0038
340.009	7.7897	76.0004	0.0035
340.009	7.7897	76.0001	0.0036
340.008	7.7896	75.9992	0.0032
340.007	5.9323	58.1965	0.0025
340.007	5.9323	58.1955	0.0010
340.010	5.9324	58.1962	0.0017
340.010	5.9324	58.1962	0.0020

TABLE 5 (*continued*)

T/K	p/MPa	ρ_{exp}/(kg · m^{-3})	$10^2(\rho_{exp} - \rho_{EOS})/\rho_{EOS}$
340.007	3.8746	38.1897	−0.0054
340.010	3.8746	38.1894	−0.0058
340.009	3.8746	38.1896	−0.0061
340.007	3.8746	38.1898	−0.0057
340.008	3.8746	38.1897	−0.0056
340.010	3.8746	38.1895	−0.0060

Measurements along isotherms with pressures measured with the pressure transducer.

Instruments model PG7601). These measurements are given in table 6. A direct connection between the densimeter and the piston gage was used; in other words, there was no pressure separating diaphragm. Such an arrangement allows the highest accuracy, but is feasible only for inert gases compatible with the piston gage and also requires considerable manual operation. The piston gage was used here to fully demonstrate the capabilities of the density system without the confounding effects of the (relatively large) uncertainties in the pressure transducers. Most of the tests used the "high-range piston" with an area of 49 mm^2 and maximum pressure of 7.0 MPa. A few tests used the "low-range piston" (980 mm^2 area and 0.35 MPa maximum pressure) or the "medium-range piston" (196 mm^2 area and 1.75 MPa maximum pressure).

4.1.3. Comparison to equation of state and literature data

The new measurements are compared to the recent, comprehensive and high-accuracy equation of state (EOS) of Span *et al.* [20] in figure 5. This equation of state is based on extensive experimental data and has an uncertainty in density of 0.02% at pressures up to 30 MPa. For temperatures between 270 K and 350 K and pressures up to 12 MPa the uncertainty of the EOS is 0.01%. The average absolute deviation for all of the present data compared to the equation of state is 0.0042%. The average absolute deviation for the points measured with the pressure transducer (0.0045%) is only slightly higher than the 0.0034% for the points measured with the piston gage. Virtually all of the present data agree with the Span equation within 0.01%, except for points at the lowest densities measured and for the high pressure points at 480 K and 500 K. The maximum deviation at 500 K and 16 MPa is 0.023%. At $T = 293$ K and $p = 0.1$ MPa where $\rho = 1.1$ kg · m^{-3}, the maximum deviation is 0.024%.

Figure 6 compares the present data to selected literature data. Span *et al.* [20] document 80 (p, ρ, T) data sets in the literature and fitted their equation of state to a subset of the 20 best sources. We compare our data with the eight literature data sets out of the 20 which overlap our temperature and pressure range. Our data are seen to agree very well with the literature data, and they exhibit considerably less scatter than the data of Duschek *et al.* [21], Jaeschke and Hinze [22], Michels *et al.* [24,25], and Otto *et al.* [27]. The data of Klimeck *et al.* [23], Nowak *et al.* [26], and Pieperbeck *et al.* [28] were given heavy

TABLE 6

Experimentally measured pressures p and densities ρ_{exp} at temperatures T for nitrogen with a comparison to the densities calculated with the equation of state of Span *et al.* [20] ρ_{EOS}

T/K	p/MPa	ρ_{exp}/(kg · m^{-3})	$10^2(\rho_{exp} - \rho_{EOS})/\rho_{EOS}$
		$T = 293$ K; *high-range piston*	
293.140	5.99427	69.2915	−0.0015
293.139	5.99425	69.2914	−0.0014
293.140	5.99424	69.2909	−0.0019
293.139	5.99423	69.2910	−0.0017
293.140	5.99422	69.2909	−0.0016
293.138	5.99422	69.2910	−0.0018
293.139	5.99421	69.2908	−0.0018
293.139	4.99516	57.7599	−0.0019
293.139	4.99515	57.7597	−0.0020
293.140	4.99513	57.7592	−0.0022
293.139	3.99606	46.1982	−0.0005
293.139	3.99606	46.1980	−0.0007
293.139	3.99605	46.1976	−0.0015
293.139	3.99605	46.1976	−0.0016
293.139	3.99605	46.1974	−0.0017
293.139	3.99605	46.1974	−0.0019
293.138	3.99605	46.1973	−0.0023
293.139	2.99707	34.6236	−0.0011
293.139	2.99706	34.6235	−0.0012
293.139	2.99706	34.6233	−0.0015
293.139	2.99705	34.6233	−0.0013
293.138	2.99705	34.6235	−0.0011
293.139	1.99801	23.0541	0.0000
293.139	1.99801	23.0541	0.0003
293.139	1.99801	23.0539	−0.0006
293.138	1.99801	23.0541	0.0000
293.139	0.99901	11.5075	0.0015
293.139	0.99901	11.5075	0.0018
293.139	0.99901	11.5074	0.0008
293.139	0.99901	11.5074	0.0008
293.139	0.99901	11.5074	0.0009
293.138	1.49850	17.2764	−0.0017
293.138	1.49850	17.2762	−0.0031
293.139	1.49849	17.2761	−0.0032
293.139	1.49849	17.2763	−0.0018
		$T = 293$ K; *mid-range piston*	
293.139	0.99900	11.5071	−0.0013
293.139	0.99899	11.5071	−0.0011
293.140	0.99899	11.5071	−0.0002
293.140	0.99899	11.5072	0.0000
293.140	0.74925	8.6261	0.0004
293.140	0.74924	8.6261	0.0004
293.140	0.74924	8.6260	−0.0005
293.140	0.74924	8.6260	−0.0001
293.140	0.74924	8.6260	0.0000
293.139	0.49949	5.7477	0.0014
293.140	0.49949	5.7477	0.0023
293.140	0.49949	5.7476	0.0008
293.139	0.49949	5.7475	−0.0013
293.139	0.29970	3.4472	0.0019
293.139	0.29970	3.4470	−0.0013
293.139	0.29970	3.4472	0.0029
293.139	0.29970	3.4472	0.0040
293.139	0.29970	3.4470	−0.0008
		$T = 293$ K; *low-range piston*	
293.139	0.29971	3.4473	0.0020
293.140	0.29971	3.4473	0.0032
293.140	0.29971	3.4472	0.0003

(*continued on next page*)

TABLE 6 (*continued*)

T/K	p/MPa	$\rho_{exp}/(kg \cdot m^{-3})$	$10^2(\rho_{exp} - \rho_{EOS})/\rho_{EOS}$
293.140	0.29971	3.4472	−0.0014
293.140	0.29971	3.4473	0.0034
293.140	0.19981	2.2978	0.0060
293.140	0.19981	2.2977	0.0025
293.140	0.19981	2.2976	0.0004
293.140	0.19981	2.2977	0.0024
293.140	0.19981	2.2978	0.0063
293.140	0.19981	2.2976	0.0011
293.140	0.09991	1.1486	0.0042
293.141	0.09991	1.1487	0.0122
293.141	0.09991	1.1485	−0.0011
293.140	0.09991	1.1488	0.0239
293.141	0.09991	1.1487	0.0168
		$T = 293$ K; *mid-range piston (replicate test)*	
293.139	1.49849	17.2763	−0.0018
293.139	1.49849	17.2763	−0.0014
293.140	1.49849	17.2761	−0.0026
293.140	1.49849	17.2762	−0.0018
293.139	1.49849	17.2763	−0.0013
		$T = 340$ K; *high-range piston*	
339.977	5.99414	58.7959	−0.0021
339.978	5.99413	58.7959	−0.0018
339.978	5.99413	58.7960	−0.0016
339.977	5.99412	58.7959	−0.0018
339.977	5.99411	58.7959	−0.0016
339.976	3.99602	39.3820	−0.0020
339.977	3.99602	39.3819	−0.0019
339.977	3.99602	39.3818	−0.0019
339.977	3.99602	39.3818	−0.0019
339.977	3.99601	39.3817	−0.0022
339.975	1.99798	19.7585	−0.0006
339.975	1.99798	19.7583	−0.0017
339.976	1.99798	19.7583	−0.0014
339.976	1.99798	19.7583	−0.0013
339.977	1.99797	19.7584	−0.0005
339.976	0.99901	9.8916	0.0006
339.976	0.99901	9.8915	−0.0007
339.976	0.99900	9.8915	0.0002
339.977	0.99900	9.8915	0.0004
339.977	0.99900	9.8916	0.0012
339.975	0.49950	4.9482	0.0017
339.975	0.49950	4.9481	−0.0002
339.975	0.49950	4.9482	0.0021
339.976	0.49950	4.9481	−0.0010
339.975	0.49950	4.9480	−0.0017
		$T = 400$ K; *high-range piston*	
399.973	5.99409	49.4947	−0.0011
399.973	5.99408	49.4948	−0.0008
399.973	5.99407	49.4948	−0.0007
399.973	5.99407	49.4949	−0.0006
399.973	3.99599	33.2413	−0.0005
399.974	3.99599	33.2410	−0.0012
399.974	3.99599	33.2411	−0.0008
399.973	3.99599	33.2410	−0.0011
399.973	3.99599	33.2410	−0.0013
399.973	1.99797	16.7313	−0.0016
399.973	1.99797	16.7315	−0.0006
399.972	1.99797	16.7314	−0.0014
399.973	1.99797	16.7315	−0.0007
399.974	1.99797	16.7314	−0.0008
399.972	0.99899	8.3914	0.0010
399.972	0.99899	8.3913	−0.0004

TABLE 6 (*continued*)

T/K	p/MPa	$\rho_{exp}/(kg \cdot m^{-3})$	$10^2(\rho_{exp} - \rho_{EOS})/\rho_{EOS}$
399.973	0.99899	8.3912	−0.0006
399.974	0.99899	8.3913	0.0003
399.973	0.49949	4.2016	−0.0034
399.973	0.49949	4.2016	−0.0022
399.973	0.49949	4.2015	−0.0047
399.973	0.49949	4.2015	−0.0040
399.973	0.49949	4.2014	−0.0076
		$T = 440$ K; *high-range piston*	
439.982	5.99392	44.8531	0.0048
439.983	5.99392	44.8534	0.0056
439.983	5.99392	44.8532	0.0051
439.983	5.99392	44.8530	0.0047
439.979	3.99592	30.1496	0.0058
439.980	3.99592	30.1495	0.0057
439.980	3.99592	30.1492	0.0048
439.980	3.99592	30.1497	0.0063
439.979	3.99592	30.1496	0.0059
439.978	1.99796	15.1914	0.0041
439.978	1.99796	15.1913	0.0037
439.977	1.99796	15.1913	0.0037
439.977	1.99796	15.1914	0.0046
439.978	1.99796	15.1913	0.0041
439.977	0.99898	7.6237	0.0069
439.978	0.99898	7.6237	0.0069
439.978	0.99898	7.6236	0.0057
439.978	0.99898	7.6238	0.0087
439.977	0.99898	7.6237	0.0066
439.977	0.49949	3.8187	0.0094
439.978	0.49949	3.8188	0.0122
439.977	0.49949	3.8186	0.0064
439.978	0.49949	3.8187	0.0100
439.978	0.49949	3.8185	0.0047
		$T = 480$ K; *high-range piston*	
480.003	5.99406	41.0449	0.0109
480.004	5.99405	41.0443	0.0097
480.005	5.99405	41.0450	0.0118
480.005	5.99404	41.0450	0.0118
480.004	5.99404	41.0449	0.0115
480.003	3.99599	27.6009	0.0108
480.003	3.99598	27.6012	0.0115
480.003	3.99598	27.6015	0.0130
480.001	1.99800	13.9142	0.0010
480.001	1.99800	13.9139	−0.0015
480.001	1.99799	13.9149	0.0062
480.001	1.99799	13.9143	0.0020
480.002	1.99799	13.9150	0.0072
480.002	0.99899	6.9857	0.0113
480.003	0.99899	6.9852	0.0050
480.003	0.99899	6.9854	0.0075
480.003	0.99899	6.9853	0.0070
480.002	0.99899	6.9856	0.0106
480.002	0.49950	3.4996	0.0076
480.002	0.49950	3.4991	−0.0050
480.003	0.49950	3.4995	0.0054
480.004	0.49950	3.4998	0.0158
480.004	0.49950	3.4995	0.0056

Measurements along isotherms with pressures measured with the piston gage.

weight in the equation of state fit, and these sets are fitted nearly exactly by the model (average absolute deviations of 0.0040% or less).

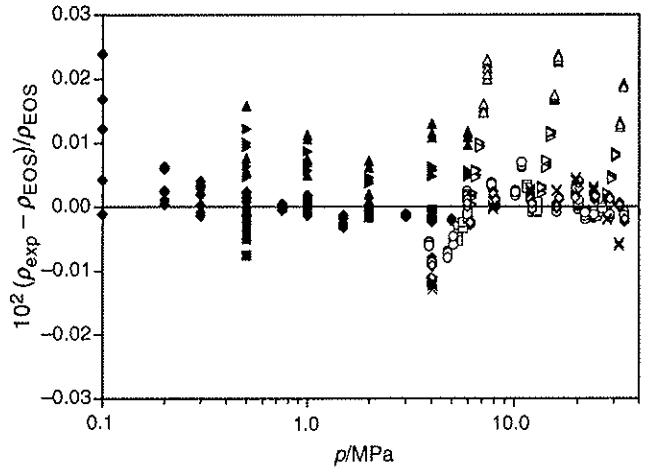

FIGURE 5. Comparison of densities measured for nitrogen ρ_{exp} with those calculated with the equation of state of Span *et al.* [20] ρ_{EOS} plotted *versus* pressure p at temperatures: ×, 250 K; ◆, 273 K to 293 K; ●, 320 K to 340 K; ■, 360 K to 400 K; ▶, 420 K to 460 K; ▲, 480 K to 500 K. Open and closed symbols are for measurements with the pressure transducer and piston gage, respectively.

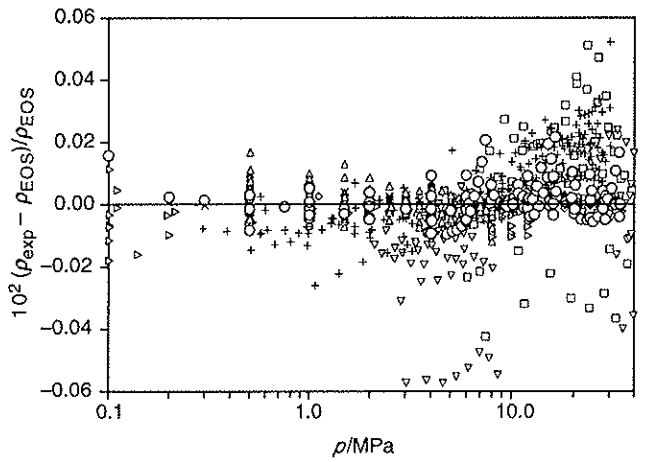

FIGURE 6. Comparison of densities measured for nitrogen with the literature values; ○, present data; △, Duschek *et al.* [21]; +, Jaeschke and Hinze [22]; ◇, Klimeck *et al.* [23]; ▽, Michels *et al.* [24,25]; ×, Nowak *et al.* [26]; □, Otto *et al.* [27]; ▷, Pieperbeck *et al.* [28]. The baseline is the equation of state of Span *et al.* [20]. For clarity, only one replicate is shown for each of the 103 state points measured here, and only about 1/4 of the points measured by Jaeschke and Hinze are shown.

4.2. Helium

Although the above comparisons show excellent agreement of our nitrogen data with the best literature values, this is not proof that they are correct. Measurements on helium allow a comparison with *ab initio* calculations of the virial coefficients. Because of the simplicity of the helium atom, the second virial coefficient has been computed nearly exactly.

4.2.1. Sample

The sample used was research-grade helium (Scott Specialty Gases). The supplier's analysis indicated impurities

TABLE 7
Experimentally measured pressures p_{exp} and densities ρ_{exp} at temperatures T for helium with a comparison to the pressures calculated with the virial model (equation (7)) p_{virial} with B,C,D determined from the present data

T/K	p_{exp}/MPa	ρ_{exp}/(kg·m^{-3})	$10^2(p_{exp} - p_{virial})/p_{virial}$
		$T = 223.15$ K	
223.1527	38.2840	66.6160	−0.0005
223.1523	38.2831	66.6140	0.0010
223.1520	38.2823	66.6131	0.0006
223.1524	38.2819	66.6126	0.0003
223.1526	38.2812	66.6119	−0.0002
223.1514	32.0166	57.4698	−0.0002
223.1523	32.0158	57.4684	−0.0003
223.1513	32.0152	57.4679	−0.0006
223.1521	32.0148	57.4668	0.0002
223.1534	32.0144	57.4666	−0.0011
223.1510	26.0250	48.1887	−0.0005
223.1525	26.0252	48.1886	−0.0001
223.1519	26.0248	48.1881	−0.0005
223.1530	26.0241	48.1868	−0.0003
223.1519	26.0237	48.1863	−0.0002
223.1502	19.6417	37.6511	−0.0005
223.1516	19.6418	37.6507	0.0007
223.1519	19.6415	37.6502	0.0004
223.1533	19.6415	37.6500	0.0003
223.1516	15.8276	30.9995	−0.0001
223.1521	15.8276	30.9993	0.0002
223.1533	15.8275	30.9990	0.0005
223.1533	15.8275	30.9989	0.0003
223.1521	15.8273	30.9985	0.0011
223.1516	11.8802	23.8089	−0.0017
223.1521	11.8803	23.8088	−0.0013
223.1531	11.8803	23.8087	−0.0011
223.1524	11.8802	23.8086	−0.0010
223.1521	11.8801	23.8085	−0.0009
223.1513	8.1331	16.6701	−0.0036
223.1529	8.1332	16.6701	−0.0037
223.1526	8.1331	16.6699	−0.0027
223.1520	8.1331	16.6700	−0.0034
223.1528	8.1332	16.6699	−0.0026
223.1508	3.9700	8.3499	−0.0073
223.1513	3.9701	8.3500	−0.0052
223.1530	3.9701	8.3499	−0.0040
223.1532	3.9702	8.3499	−0.0028
223.1518	3.9701	8.3501	−0.0057
223.1515	1.8814	4.0102	−0.0145
223.1531	1.8814	4.0101	−0.0117
223.1533	1.8814	4.0101	−0.0093
223.1523	1.8814	4.0102	−0.0113
223.1528	1.8815	4.0102	−0.0103
		$T = 253.15$ K	
253.1484	37.8169	59.5703	0.0001
253.1493	37.8158	59.5686	0.0003
253.1494	37.8148	59.5673	0.0002
253.1484	37.8137	59.5664	−0.0005
253.1490	37.8129	59.5651	−0.0003

(*continued on next page*)

TABLE 7 (*continued*)

T/K	p_{exp}/MPa	ρ_{exp}/(kg · m^{-3})	$10^2(p_{exp} - p_{virial})/p_{virial}$
253.1471	31.9403	51.6470	−0.0001
253.1486	31.9399	51.6462	0.0002
253.1498	31.9395	51.6454	0.0002
253.1483	31.9385	51.6443	0.0002
253.1479	31.9380	51.6436	0.0002
253.1481	25.9777	43.1810	−0.0016
253.1486	25.9775	43.1801	−0.0003
253.1492	25.9772	43.1796	−0.0004
253.1486	25.9769	43.1790	0.0002
253.1488	25.9765	43.1785	0.0001
253.1469	19.8657	34.0081	−0.0004
253.1478	19.8655	34.0112	−0.0119
253.1490	19.8654	34.0070	0.0007
253.1483	19.8649	34.0064	0.0008
253.1481	15.9577	27.8557	−0.0005
253.1484	15.9576	27.8555	−0.0001
253.1494	15.9576	27.8552	0.0006
253.1493	15.9575	27.8548	0.0014
253.1483	15.9573	27.8548	0.0007
253.1476	11.8955	21.2023	−0.0007
253.1493	11.8956	21.2022	−0.0003
253.1494	11.8955	21.2019	0.0004
253.1478	11.8953	21.2020	−0.0008
253.1492	11.8953	21.2018	−0.0001
253.1490	7.4723	13.6340	−0.0013
253.1480	7.4722	13.6340	−0.0018
253.1493	7.4723	13.6340	−0.0015
253.1498	7.4723	13.6340	−0.0019
253.1479	3.7846	7.0460	−0.0044
253.1487	3.7846	7.0462	−0.0073
253.1491	3.7846	7.0460	−0.0040
253.1493	3.7846	7.0461	−0.0054
253.1499	1.9292	3.6290	−0.0018
253.1502	1.9292	3.6292	−0.0078
253.1487	1.9293	3.6290	0.0001
253.1494	1.9293	3.6294	−0.0102
253.1507	1.9293	3.6292	−0.0049
		$T = 273.16$ K, *replicate 1*	
273.1615	38.1160	56.3350	0.0000
273.1618	38.1155	56.3346	−0.0006
273.1628	38.1149	56.3338	−0.0010
273.1623	38.1143	56.3327	0.0000
273.1612	38.1137	56.3321	0.0002
273.1611	31.5777	47.9581	−0.0017
273.1621	31.5775	47.9577	−0.0016
273.1624	31.5770	47.9575	−0.0028
273.1617	31.5766	47.9570	−0.0028
273.1618	31.5764	47.9567	−0.0025
273.1627	25.9657	40.4020	−0.0027
273.1623	25.9652	40.4011	−0.0023
273.1609	25.9649	40.4011	−0.0027
273.1623	25.9649	40.4013	−0.0037
273.1623	25.9645	40.3998	−0.0012

TABLE 7 (*continued*)

T/K	p_{exp}/MPa	ρ_{exp}/(kg · m^{-3})	$10^2(p_{exp} - p_{virial})/p_{virial}$
273.1620	19.7090	31.5386	−0.0012
273.1605	19.7087	31.5382	−0.0009
273.1610	19.7087	31.5385	−0.0023
273.1617	19.7083	31.5379	−0.0022
273.1614	19.7083	31.5381	−0.0030
273.1591	15.5864	25.4234	−0.0018
273.1611	15.5866	25.4235	−0.0021
273.1614	15.5866	25.4235	−0.0019
273.1621	15.5866	25.4232	−0.0012
273.1616	15.5865	25.4233	−0.0017
273.1596	12.0563	19.9988	−0.0037
273.1610	12.0564	19.9990	−0.0045
273.1612	12.0564	19.9987	−0.0031
273.1629	12.0565	19.9988	−0.0036
273.1631	12.0564	19.9985	−0.0027
273.1597	7.7666	13.1563	−0.0054
273.1604	7.7661	13.1555	−0.0051
273.1622	7.7657	13.1545	−0.0037
273.1611	7.7653	13.1538	−0.0029
273.1605	7.7649	13.1534	−0.0050
273.1604	3.6268	6.2735	−0.0133
273.1604	3.6267	6.2732	−0.0105
273.1620	3.6266	6.2731	−0.0111
273.1617	3.6266	6.2730	−0.0104
273.1606	3.6266	6.2730	−0.0095
		$T = 273.16$ K, *replicate 2*	
273.1590	37.2012	55.1895	−0.0005
273.1601	37.2006	55.1885	−0.0004
273.1602	37.1998	55.1874	−0.0002
273.1599	37.1990	55.1865	−0.0004
273.1612	37.1978	55.1850	−0.0007
273.1612	32.2132	48.7913	−0.0005
273.1606	32.2125	48.7903	0.0001
273.1623	32.2115	48.7886	0.0003
273.1617	32.2108	48.7880	−0.0003
273.1609	32.2101	48.7873	−0.0004
273.1603	25.4352	39.6682	0.0003
273.1619	25.4350	39.6678	0.0000
273.1621	25.4345	39.6672	−0.0002
273.1613	25.4341	39.6666	0.0003
273.1615	25.4338	39.6662	0.0001
273.1620	19.6452	31.4453	−0.0001
273.1614	19.6449	31.4450	−0.0002
273.1615	19.6448	31.4447	0.0001
273.1621	19.6446	31.4443	0.0005
273.1607	15.9805	26.0175	−0.0002
273.1617	15.9805	26.0174	−0.0005
273.1618	15.9802	26.0170	−0.0005
273.1612	15.9801	26.0168	−0.0004
273.1624	15.9800	26.0165	0.0001
273.1599	11.7834	19.5715	−0.0018
273.1600	11.7833	19.5714	−0.0020
273.1610	11.7833	19.5712	−0.0015
273.1615	11.7833	19.5710	−0.0011
273.1606	11.7832	19.5710	−0.0014

TABLE 7 (*continued*)

T/K	p_{exp}/MPa	ρ_{exp}/(kg · m^{-3})	$10^2(p_{exp} - p_{virial})/p_{virial}$
273.1602	7.9161	13.3992	−0.0023
273.1617	7.9161	13.3990	−0.0007
273.1623	7.9161	13.3991	−0.0023
273.1610	7.9160	13.3990	−0.0016
273.1606	7.9160	13.3990	−0.0020
273.1599	3.9528	6.8257	−0.0070
273.1606	3.9528	6.8257	−0.0064
273.1611	3.9529	6.8257	−0.0056
273.1620	3.9529	6.8257	−0.0044
273.1616	3.9529	6.8257	−0.0051
273.1618	1.9564	3.4135	−0.0171
273.1606	1.9564	3.4135	−0.0156
273.1615	1.9565	3.4135	−0.0147
273.1623	1.9565	3.4135	−0.0148
273.1616	1.9565	3.4134	−0.0122
		$T = 273.16$ K, *replicate 3*	
273.1635	37.5197	55.5878	0.0014
273.1617	37.5177	55.5858	0.0010
273.1614	37.5166	55.5843	0.0013
273.1618	37.5154	55.5829	0.0010
273.1613	37.5143	55.5816	0.0011
273.1598	31.86702	48.3375	0.0012
273.1603	31.8667	48.3368	0.0011
273.1608	31.8661	48.3358	0.0013
273.1594	31.8654	48.3352	0.0011
273.1599	31.8648	48.3344	0.0009
273.1601	25.9160	40.3324	0.0013
273.1606	25.9157	40.3317	0.0016
273.1608	25.9154	40.3313	0.0014
273.1602	25.9149	40.3307	0.0016
273.1602	25.9146	40.3302	0.0019
273.1585	20.2431	32.3140	0.0011
273.1598	20.2425	32.3130	0.0013
273.1607	20.2422	32.3124	0.0014
273.1601	20.2420	32.3121	0.0015
273.1608	20.2418	32.3117	0.0018
273.1602	16.0904	26.1826	0.0014
273.1615	16.0904	26.1823	0.0018
273.1612	16.0902	26.1822	0.0014
273.1608	16.0901	26.1821	0.0011
273.1614	16.0900	26.1818	0.0014
273.1610	11.8299	19.6438	0.0005
273.1606	11.8298	19.6436	0.0010
273.1611	11.8298	19.6435	0.0011
273.1614	11.8298	19.6435	0.0013
273.1611	11.8297	19.6434	0.0009
273.1601	8.0061	13.5452	0.0003
273.1605	8.0062	13.5452	0.0006
273.1610	8.0061	13.5452	0.0003
273.1612	8.0061	13.5452	−0.0001
273.1609	8.0061	13.5452	−0.0003
273.1608	3.9261	6.7802	−0.0016
273.1621	3.9262	6.7804	−0.0043
273.1628	3.9262	6.7802	−0.0011
273.1622	3.9262	6.7802	−0.0012
273.1623	3.9262	6.7803	−0.0024

TABLE 7 (*continued*)

T/K	p_{exp}/MPa	ρ_{exp}/(kg · m^{-3})	$10^2(p_{exp} - p_{virial})/p_{virial}$
273.1613	1.8818	3.2839	0.0040
273.1626	1.8818	3.2839	0.0030
273.1631	1.8818	3.2839	0.0035
273.1621	1.8818	3.2839	0.0034
273.1623	1.8818	3.2839	0.0041
		$T = 273.16$ K, *replicate 4*	
273.1611	37.5396	55.6136	0.0006
273.1616	37.5386	55.6125	0.0001
273.1613	37.5374	55.6109	0.0004
273.1609	37.5361	55.6095	0.0001
273.1610	37.5312	55.6035	−0.0004
273.1575	31.7799	48.2235	0.0004
273.1613	31.7788	48.2215	0.0005
273.1601	31.7775	48.2200	0.0003
273.1616	31.7768	48.2188	0.0006
273.1615	31.7760	48.2177	0.0005
273.1607	31.7750	48.2167	0.0004
273.1610	25.4665	39.7113	0.0009
273.1608	25.4661	39.7107	0.0008
273.1611	25.4655	39.7099	0.0009
273.1612	25.4650	39.7092	0.0007
273.1609	25.4644	39.7083	0.0011
273.1600	19.8702	31.7727	0.0010
273.1617	19.8701	31.7722	0.0013
273.1613	19.8697	31.7718	0.0011
273.1612	19.8694	31.7712	0.0016
273.1619	19.8692	31.7709	0.0013
273.1600	16.0780	26.1640	0.0007
273.1604	16.0777	26.1636	0.0008
273.1612	16.0776	26.1633	0.0009
273.1611	16.0774	26.1631	0.0007
273.1608	16.0773	26.1628	0.0012
273.1607	11.8551	19.6835	−0.0005
273.1599	11.8550	19.6833	−0.0003
273.1608	11.8549	19.6831	−0.0002
273.1603	11.8549	19.6832	−0.0005
273.1613	11.8550	19.6831	0.0002
273.1602	7.9734	13.4923	−0.0018
273.1616	7.9734	13.4922	−0.0014
273.1608	7.9734	13.4922	−0.0016
273.1612	7.9734	13.4921	−0.0011
273.1614	7.9733	13.4919	0.0002
273.1594	3.9751	6.8634	−0.0056
273.1607	3.9752	6.8635	−0.0063
273.1615	3.9752	6.8635	−0.0062
273.1613	3.9752	6.8633	−0.0034
273.1606	3.9752	6.8633	−0.0029
273.1587	1.9273	3.3630	−0.0095
273.1598	1.9273	3.3629	−0.0053
273.1612	1.9274	3.3630	−0.0061
273.1614	1.9274	3.3629	−0.0029
273.1609	1.9274	3.3629	−0.0035

(*continued on next page*)

TABLE 7 (*continued*)

T/K	p_{exp}/MPa	ρ_{exp}/(kg · m^{-3})	$10^2(p_{exp} - p_{virial})/p_{virial}$
273.1594	0.9358	1.6415	−0.0171
273.1604	0.9359	1.6416	−0.0200
273.1619	0.9359	1.6416	−0.0163
273.1609	0.9359	1.6415	−0.0094
273.1616	0.9359	1.6416	−0.0128
	$T = 293.15$ K, *replicate 1, 99.999% sample*		
293.1521	29.5108	42.5405	0.0046
293.1525	29.5100	42.5394	0.0050
293.1519	29.5096	42.5393	0.0041
293.1529	29.5093	42.5383	0.0054
293.1524	29.5090	42.5383	0.0044
293.1522	29.5084	42.5375	0.0044
293.1523	29.5081	42.5373	0.0042
293.1520	29.5072	42.5361	0.0044
293.1528	24.4758	36.0152	0.0040
293.1535	24.4751	36.0141	0.0044
293.1522	24.4749	36.0141	0.0041
293.1535	24.4747	36.0137	0.0038
293.1524	24.4742	36.0133	0.0035
293.1532	24.4739	36.0123	0.0048
293.1521	24.4736	36.0124	0.0039
293.1542	24.4735	36.0121	0.0035
293.1525	18.0192	27.2484	0.0032
293.1531	18.0191	27.2483	0.0028
293.1536	18.0190	27.2479	0.0034
293.1530	18.0188	27.2477	0.0032
293.1544	18.0187	27.2474	0.0038
293.1526	18.0185	27.2473	0.0032
293.1527	18.0181	27.2468	0.0035
293.1527	18.0181	27.2464	0.0046
293.1538	14.0183	21.5716	0.0042
293.1528	14.0182	21.5716	0.0041
293.1545	14.0182	21.5715	0.0039
293.1520	14.0181	21.5714	0.0041
293.1524	14.0181	21.5712	0.0051
293.1534	14.0180	21.5709	0.0054
293.1524	14.0179	21.5709	0.0050
293.1539	14.0178	21.5709	0.0042
293.1538	10.0348	15.7205	−0.0001
293.1536	10.0347	15.7202	0.0011
293.1525	10.0347	15.7202	0.0014
293.1531	10.0346	15.7202	0.0002
293.1535	10.0345	15.7199	0.0008
293.1551	10.0342	15.7195	−0.0003
293.1525	7.0582	11.2089	0.0034
293.1514	7.0581	11.2089	0.0024
293.1526	7.0581	11.2088	0.0030
293.1517	7.0580	11.2086	0.0039
293.1525	7.0580	11.2086	0.0030
293.1516	4.0070	6.4543	0.0137
293.1535	4.0070	6.4543	0.0121
293.1519	4.0070	6.4543	0.0121
293.1508	4.0069	6.4542	0.0129
293.1537	4.0070	6.4542	0.0130
293.1529	4.0069	6.4542	0.0125
293.1503	4.0070	6.4541	0.0152

TABLE 7 (*continued*)

T/K	p_{exp}/MPa	ρ_{exp}/(kg · m^{-3})	$10^2(p_{exp} - p_{virial})/p_{virial}$
	$T = 293.15$ K, *replicate 2*		
293.1509	38.0072	52.9958	−0.0041
293.1516	38.0061	52.9944	−0.0040
293.1524	38.0054	52.9930	−0.0030
293.1521	38.0044	52.9921	−0.0036
293.1519	38.0034	52.9909	−0.0035
293.1508	31.8501	45.4879	−0.0014
293.1505	31.8482	45.4862	−0.0032
293.1520	31.8475	45.4845	−0.0014
293.1524	31.8469	45.4837	−0.0015
293.1516	31.8462	45.4829	−0.0016
293.1521	25.7791	37.7309	−0.0012
293.1511	25.7785	37.7301	−0.0009
293.1515	25.7782	37.7298	−0.0015
293.1525	25.7778	37.7293	−0.0018
293.1519	25.7773	37.7285	−0.0011
293.1512	19.9058	29.8599	−0.0016
293.1508	19.9057	29.8595	−0.0008
293.1522	19.9056	29.8592	−0.0006
293.1524	19.9054	29.8588	−0.0002
293.1516	19.9050	29.8586	−0.0013
293.1513	16.0049	24.4156	−0.0007
293.1519	16.0048	24.4153	−0.0005
293.1527	16.0047	24.4152	−0.0005
293.1521	16.0051	24.4159	−0.0012
293.1514	16.0045	24.4152	−0.0013
293.1493	11.7621	18.2839	−0.0030
293.1511	11.7621	18.2839	−0.0035
293.1513	11.7621	18.2837	−0.0028
293.1523	11.7620	18.2835	−0.0028
293.1518	11.7619	18.2834	−0.0030
293.1509	7.8830	12.4722	−0.0056
293.1522	7.8826	12.4715	−0.0054
293.1531	7.8821	12.4707	−0.0053
293.1519	7.8816	12.4701	−0.0063
293.1514	7.8813	12.4696	−0.0054
293.1511	3.9089	6.3008	−0.0130
293.1518	3.9089	6.3007	−0.0125
293.1530	3.9089	6.3007	−0.0124
293.1514	3.9089	6.3009	−0.0152
293.1525	3.9089	6.3006	−0.0101
293.1509	1.7316	2.8204	−0.0188
293.1516	1.7316	2.8205	−0.0196
293.1516	1.7316	2.8205	−0.0211
293.1530	1.7316	2.8204	−0.0184
293.1523	1.7316	2.8207	−0.0292
293.1513	0.9801	1.6025	−0.0376
293.1514	0.9802	1.6025	−0.0334
293.1525	0.9802	1.6025	−0.0313
293.1516	0.9802	1.6025	−0.0266
293.1525	0.9802	1.6026	−0.0331
		$T = 323.15$ K	
323.1499	37.8920	48.6904	−0.0003
323.1498	37.8906	48.6888	−0.0003
323.1502	37.8896	48.6876	−0.0003

TABLE 7 (*continued*)

T/K	p_{exp}/MPa	ρ_{exp}/(kg · m^{-3})	$10^2(p_{exp} - p_{virial})/p_{virial}$
323.1506	37.8886	48.6863	0.0000
323.1508	37.8877	48.6852	0.0002
323.1503	31.7973	41.7543	0.0003
323.1502	31.7967	41.7536	0.0004
323.1513	31.7961	41.7528	0.0004
323.1515	31.7954	41.7520	0.0003
323.1508	31.7948	41.7513	0.0003
323.1511	25.6804	34.4895	−0.0004
323.1504	25.6800	34.4890	−0.0003
323.1503	25.6796	34.4886	−0.0004
323.1513	25.6793	34.4883	−0.0008
323.1511	25.6788	34.4876	−0.0006
323.1477	19.3062	26.5662	0.0000
323.1490	19.3055	26.5653	0.0000
323.1494	19.3054	26.5650	0.0004
323.1509	19.3053	26.5647	0.0004
323.1506	19.3050	26.5643	0.0009
323.1478	15.0820	21.1007	0.0000
323.1495	15.0816	21.1001	0.0003
323.1497	15.0815	21.1000	−0.0001
323.1503	15.0814	21.0997	0.0007
323.1501	15.0813	21.0997	−0.0001
323.1491	11.6483	16.5232	−0.0012
323.1490	11.6482	16.5230	−0.0006
323.1506	11.6482	16.5228	0.0000
323.1508	11.6481	16.5227	−0.0002
323.1494	11.6479	16.5226	−0.0009
323.1492	7.9744	11.4837	−0.0027
323.1493	7.9744	11.4836	−0.0012
323.1502	7.9744	11.4836	−0.0014
323.1499	7.9743	11.4836	−0.0022
323.1495	7.9743	11.4834	−0.0008
323.1491	3.9591	5.7989	−0.0117
323.1498	3.9591	5.7989	−0.0107
323.1509	3.9591	5.7989	−0.0120
323.1504	3.9591	5.7987	−0.0076
323.1495	3.9591	5.7989	−0.0109
323.1493	1.7801	2.6323	−0.0315
323.1492	1.7801	2.6324	−0.0343
323.1504	1.7801	2.6322	−0.0261
323.1506	1.7802	2.6323	−0.0288
323.1494	1.7801	2.6323	−0.0295

Measurements along isotherms with pressures measured with the pressure transducer.

of nitrogen, oxygen, and neon of 0.3 ppm to 0.4 ppm; other impurities were less than 0.1 ppm for an overall purity of 99.99987%. Based on this analysis, the molar mass of our sample was 4.002631 g · mol^{-1} or 7.3 ppm higher than the nominal value [19]. We also used helium of 99.999% purity for one set of measurements at 293.15 K.

4.2.2. Experimental results

Helium was measured along isotherms at 223.15 K and 253.15 K, four series at 273.16 K, two series at 293.15 K and 323.15 K. Each isotherm started at a pressure of 30 MPa to 38 MPa; eight to ten pressures were measured for each isotherm ending at 1 MPa to 4 MPa. At each pressure, five replicate density determinations were made, for a total of 411 (p, ρ, T) measurements. The data are given in table 7.

4.2.3. Comparison to ab initio calculations

Statistical mechanics provides that gases at low densities obey a simple virial expansion:

$$p = RT\rho(1 + B\rho + C\rho^2 + D\rho^3 + \cdots), \quad (7)$$

where T is temperature, R is the gas constant, ρ is density, and B, C, and D are the virial coefficients. This can be rearranged to

$$\frac{Z-1}{\rho} = B + C\rho + D\rho^2 + \cdots, \quad (8)$$

where the compressibility $Z = p/RT\rho$, so that a plot of $(Z-1)/\rho$ *versus* ρ should be a line with an intercept equal to B and an initial slope equal to C. At higher pressures and densities, the fourth virial is revealed by curvature in the plot. The data were fitted to equation (8) by an orthogonal distance regression using the package ODRPACK [29]. (Orthogonal distance regression allows for uncertainties in both the independent and dependent variables; in contrast, ordinary least squares assumes all uncertainties are in the dependent variable.) The data were weighted by $1/u^2$, and any points that differed by more than 2σ from the fit were given zero weight. The fitted virial coefficients are given in table 8. The virial coefficients for each of the nitrogen isotherms measured with the piston gage are also given in table 8. The uncertainty in the helium virials are based on a pressure uncertainty of (0.0051% + 0.4 kPa). This is smaller than the uncertainty stated in section 3, and it is justified because the pressure transducer was

TABLE 8
Experimentally determined virial coefficients B, C, and D for helium and nitrogen at temperatures T; uncertainties u are for $k = 2$

T/K	B/(cm^3 · mol^{-1})	$u(B)$	C/(cm^6 · mol^{-2})	$u(C)$	D/(cm^9 · mol^{-3})	$u(D)$
			Helium			
223.152	12.091	0.049	122.93	5.56	980	188
253.149	11.996	0.039	116.17	4.53	899	160
273.161	11.926	0.032	111.02	3.67	915	130
273.161	11.916	0.034	113.92	4.09	759	148
273.161	11.926	0.031	112.27	3.49	829	121
273.161	11.920	0.036	113.39	4.51	776	167
293.153	11.863	0.041	106.20	6.04	941	270
293.152	11.828	0.038	112.29	5.25	620	210
323.150	11.719	0.045	105.50	6.30	652	266
			Nitrogen			
293.139	−5.94	0.07	1466	23		
339.976	2.07	0.12	1363	42		
399.973	9.17	0.26	1278	107		
439.979	12.51	0.38	1298	177		
480.003	15.18	0.47	1322	226		

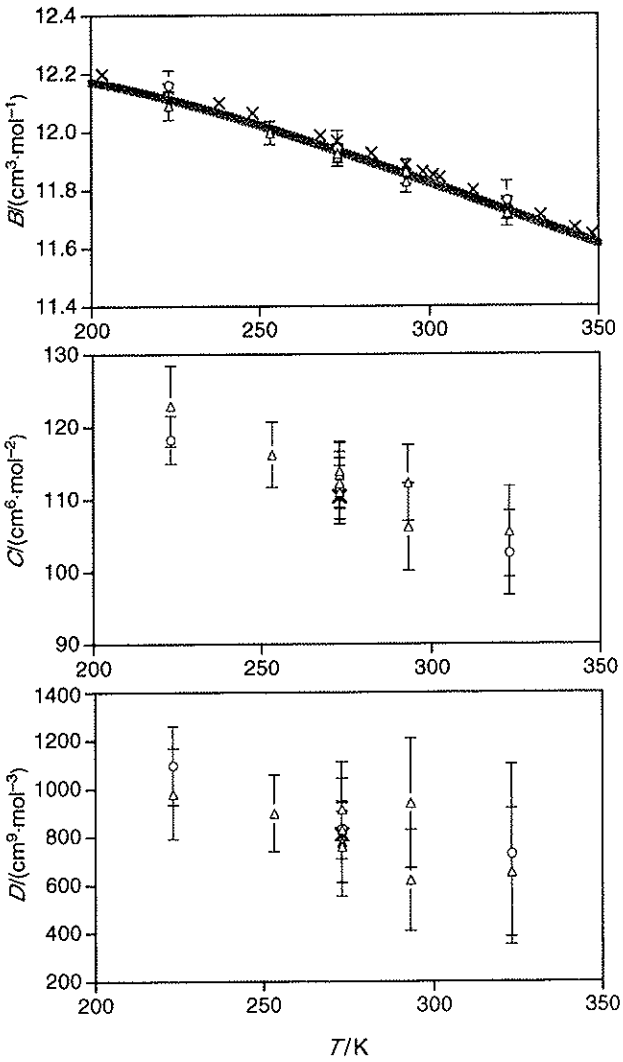

FIGURE 7. Virial coefficients for helium; △, present data; ○, Blancett *et al.* [32]; ×, Gammon [31]; and line, *ab initio* calculations of Hurly and Moldover [30]. The error bars represent $k = 2$ uncertainties for the present data and the data of Blancett *et al.*, and the width of the line approximates the uncertainty in the *ab initio* values.

calibrated immediately before and after the helium measurements, and the zero drift was checked between each isotherm.

Figure 7 compares the present virial coefficients with the *ab initio* calculations of Hurly and Moldover [30]. Also shown are two other experimental sources from the literature. The present results show excellent agreement with the theoretical values and also the experimental values of Gammon [31], and Blancett *et al.* [32]. These references were identified by Hurly and Moldover [30] and Moldover [33] as the most reliable literature sources. The differences are well within the mutual uncertainties, except that the second virials of Gammon are just outside the uncertainties of the *ab initio* calculations. (The error bars for the Gammon *B* values are the same size as the plot symbols, but Hurly and Moldover [30] state that Gammon did not include all error sources in his uncertainty statement.) It

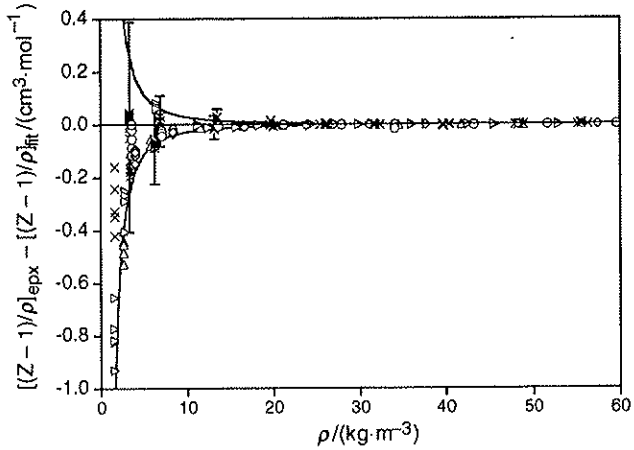

FIGURE 8. Deviations of experimental helium data with the virial model (equation (8)) as a function of density ρ at temperatures: ◇, 223 K; ○, 253 K; ×, 273 K; ▶, 293 K; ▲, 323 K. Error bars ($k = 2$) are shown for selected points at 273 K; at densities greater than 20 kg · m^{-3} the error bars are smaller than the plot symbols. The solid lines represents the effect of a systematic error of ±0.0006 kg · m^{-3} in density or ±0.4 kPa in pressure.

is also worthwhile to note that this agreement applies between theoretical calculations and three completely different experimental techniques: Blancett used a Burnett expansion technique and Gammon derived virial coefficients from speed of sound measurements.

Deviations of the experimental data from equation (8) are shown in figure 8. This type of plot accentuates any systematic deviations, and, indeed, a significant negative deviation is observed at densities below about 15 kg · m^{-3}. The effect of a systematic error in density of 0.0006 kg · m^{-3} (corresponding to 6 μg in the sinker weighings) or a systematic error in pressure of 0.4 kPa are virtually the same, and are shown as the solid lines in figure 8. Either effect would explain the observed deviations. The estimated uncertainties in temperature and sinker volume result in errors in $(Z - 1)/\rho$ that are much smaller than the pressure and weighing effects plotted. This analysis does reveal systematic errors in the densimeter and suggests their cause(s), but it also demonstrates that the uncertainty estimates presented in section 3 are reasonable.

The final column in table 7 presents deviations of the measured pressures with those calculated from equation (7). For the replicate isotherms, the average values for the virial coefficients at each temperature are used. The replicate isotherms represent different fillings of helium on different days, and they indicate the high repeatability of the densimeter. For example, for the 20 replicate points at 273.16 K and 37 MPa to 38 MPa the deviations from the virial fit range from −0.0010% to +0.0014%; these represent four different fillings of helium.

4.3. High-density fluoroether

Densities were measured for liquid 2-trifluoromethyl-3-ethoxydodecafluorohexane ($C_9F_{15}H_5O$, also known as HFE-7500). These measurements were performed primarily

TABLE 9
Experimentally measured pressures p and densities ρ_{exp} at temperatures T for 2-trifluoromethyl-3-ethoxydodecafluorohexane with a comparison to the densities calculated with the empirical fit (equation (9)) ρ_{fit}

T/K	p/MPa	ρ_{exp}/(kg · m^{-3})	$10^2(\rho_{exp} - \rho_{fit})/\rho_{fit}$
285.000	10.1974	1670.467	0.0075
285.002	10.1813	1670.439	0.0080
285.000	5.2202	1659.809	−0.0013
285.002	5.2128	1659.790	−0.0013
285.001	1.2052	1650.594	−0.0067
285.002	1.2048	1650.597	−0.0063
285.002	1.2042	1650.591	−0.0066
308.003	19.8451	1649.196	−0.0017
308.007	19.8250	1649.159	−0.0010
308.008	19.7864	1649.073	−0.0011
308.012	10.4765	1628.238	0.0064
308.013	10.4677	1628.212	0.0062
308.012	10.4505	1628.167	0.0058
308.012	5.2234	1615.004	0.0001
308.012	5.2196	1614.987	−0.0003
308.014	5.2157	1614.977	−0.0001
308.012	1.3310	1604.292	−0.0003
308.012	1.3209	1604.262	−0.0003
308.013	1.3145	1604.243	−0.0002
349.999	17.0822	1568.894	0.0007
349.998	16.8503	1568.238	0.0004
349.999	16.8359	1568.197	0.0006
349.999	19.7860	1576.327	0.0024
349.999	19.7324	1576.182	0.0023
349.998	19.7158	1576.138	0.0022
349.998	10.4012	1548.708	−0.0030
349.999	10.3945	1548.686	−0.0029
349.999	10.3877	1548.662	−0.0030
349.998	5.2910	1531.029	−0.0066
349.998	5.2861	1531.011	−0.0067
349.998	1.2860	1515.323	0.0054
349.999	1.2864	1515.323	0.0054
349.998	1.2868	1515.323	0.0052
349.998	1.2867	1515.322	0.0051
349.998	1.2863	1515.321	0.0052
349.998	1.2858	1515.319	0.0052
400.003	19.5825	1488.672	0.0012
400.004	19.5599	1488.587	0.0010
400.004	19.5431	1488.527	0.0010
400.005	19.5186	1488.438	0.0009
400.004	19.4954	1488.354	0.0007
400.005	19.4163	1488.066	0.0004
400.003	19.3914	1487.975	0.0001
400.003	19.3802	1487.935	0.0001
400.004	19.3692	1487.894	0.0000
400.002	19.3471	1487.813	−0.0003
400.004	19.3282	1487.745	−0.0001
400.003	19.3173	1487.706	−0.0002
400.003	19.2867	1487.593	−0.0005
400.002	19.2756	1487.554	−0.0005
400.003	19.2576	1487.488	−0.0005
400.003	19.2177	1487.343	−0.0007
400.005	19.2075	1487.304	−0.0006
400.005	19.1970	1487.266	−0.0006
400.002	9.9841	1448.955	−0.0008
400.003	9.9797	1448.935	−0.0006
400.003	9.9756	1448.914	−0.0007
400.004	5.2288	1424.095	0.0032
400.002	5.2272	1424.086	0.0029
400.003	5.2255	1424.075	0.0030
400.002	1.1647	1398.227	−0.0048
400.003	1.1644	1398.224	−0.0046
400.004	1.1643	1398.222	−0.0045

Measurements along isotherms with pressures measured with the pressure transducer.

to provide a high-density standard for the calibration of a vibrating-tube densimeter used in another project [34]. These data demonstrate that the densimeter is capable of measuring high-density fluids, but they do not confirm the accuracy at high densities. There is no reason to believe, however, that some completely different phenomena would be present at high densities which would degrade the accuracies demonstrated above.

4.3.1. Sample

The material was supplied by the 3M Company with a stated purity of greater than 99.5%. The sample was degassed by freezing in liquid nitrogen and evacuating the vapor space, but otherwise it was used as supplied. The freeze/pump/thaw process was repeated three times until the residual pressure over the frozen sample was less than 10^{-3} Pa. A thorough analysis of the impurities would be needed before the present data could be used to develop a high-accuracy equation of state. But the present data are used primarily to demonstrate the capabilities of the densimeter, and this is not affected by sample purity.

4.3.2. Experimental results

Densities were measured along four isotherms from 285 K to 400 K with pressures to 20 MPa. The data are given in table 9 and have been fitted to the following function:

$$\rho/(\mathrm{kg\cdot m^{-3}}) = \sum_{i=1}^{2} a_i (T/100\ \mathrm{K})^{b_i} + \sum_{i=3}^{5} a_i (T/100\ \mathrm{K})^{b_i} (p/\mathrm{MPa})^{c_i}, \quad (9)$$

where the coefficients a_i, b_i, and c_i are given in table 10. The average absolute deviation is 0.0026%, and all of the data are fitted within 0.01% as shown in figure 9.

TABLE 10
Coefficients of the empirical fit of the (p, ρ, T) data for 2-trifluoromethyl-3-ethoxydodecafluorohexane (equation (9))

i	a_i	b_i	c_i
1	2123.27	−0.2	
2	−2.60204	3.2	
3	0.368290	1.55	1
4	0.00160194	5.9	1
5	−0.000427979	5.7	1.4

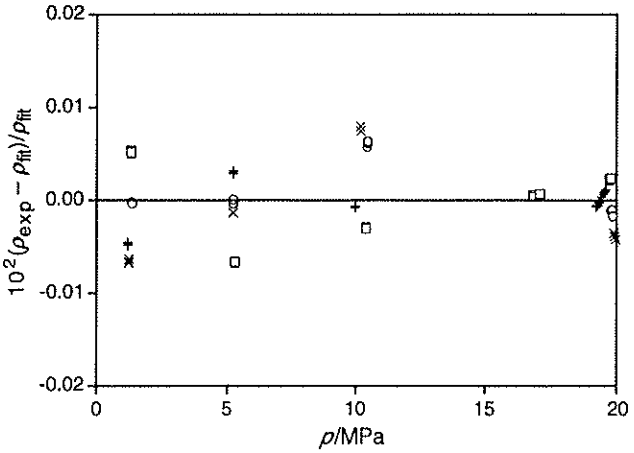

FIGURE 9. Comparison of densities ρ_{exp} measured for 2-trifluoromethyl-3-ethoxydodecafluorohexane with those calculated from the empirical fit (equation 9) ρ_{fit}; ×, 285 K; ○, 308 K; □, 350 K; +, 400 K.

Apart from a single density value at 25 °C and a linear fit for density as a function of temperature provided on the manufacturer's data sheet, these are the only known density data available for this compound.

5. Conclusions

A new instrument is described that provides an absolute determination of fluid density over wide ranges of temperature, pressure, and density. Very low uncertainties in the (p, ρ, T) data are supported by rigorous traceability and calibration procedures, by comparison to high-quality literature data, and by comparing experimental virial coefficients to those computed from *ab initio* calculations.

Acknowledgements

We express our sincere appreciation for the skilled fabrication efforts and advice on construction details provided by T. Waldorf and R. Gomez, and especially M. Rybowiak. R. Gomez calibrated the pressure transducers and assisted with the piston gage measurements. T. Bruno analyzed the purity of the nitrogen. E. Lemmon provided data files for the literature data for nitrogen and also the fit of the HFE-7500 data. This work was supported, in part, by the Division of Engineering and Geosciences, Office of Basic Energy Sciences, US Department of Energy under contract DE-AI05-88ER13823, and by NIST.

References

[1] R. Masui, K. Fujii, M. Takenaka, Metrologia 32 (1995) 333–362.
[2] R. Kleinrahm, W. Wagner, J. Chem. Thermodyn. 18 (1986) 739–760.
[3] C. Lösch-Will, Ph.D. Thesis, Lehrstuhls für Thermodynamik, Ruhr-Universität Bochum, Germany, 2005.
[4] J.G. Hust, J. Filla, D.R. Smith, J. Therm. Insul. 11 (10) (1987) 102–107.
[5] W. Wagner, K. Brachthäuser, R. Kleinrahm, H.W. Lösch, Int. J. Thermophys. 16 (1995) 399–411.
[6] R.S. Davis, Metrologia 29 (1992) 67–70.
[7] H.W. Lösch, Entwicklung und Aufbau von neuen Magnetschwebenwaagen zur berührungsfreien Messung vertikaler Kräfte, Fortschr.-Ber., Reihe 3, Number 138, VDI-Verlag, Düsseldorf, 1987.
[8] W. Wagner, R. Kleinrahm, Metrologia 41 (2004) S24–S39.
[9] M.O. McLinden, R. Kleinrahm, W. Wagner, Int. J. Thermophys. (submitted for publication), also presented at 16th Symp. on Thermophysical Properties, Boulder, CO, 30 July–4 August, preprint posted at: ftp://ftp.boulder.nist.gov/pub/fluids/apparatus/pVT/force transmission errors.pdf.
[10] H.A. Bowman, R.M. Schnoonover, C.L. Carroll, J. Res. NBS 78A (1973) 13–40.
[11] H.A. Bowman, R.M. Schnoonover, C.L. Carroll, Metrologia 10 (1974) 117–121.
[12] Z.J. Jabbour, Report of Calibration, NIST Test Number 822/6654-00, National Institute of Standards and Technology, Gaithersburg, MD, 2000.
[13] C.A. Swenson, J. Phys. Chem. Ref. Data 12 (1983) 179–182.
[14] Y.S. Touloukian, R.K. Kirby, R.E. Taylor, P.D. Desai, Thermophysical Properties of Matter. Part 1Thermal Expansion: Metallic Elements and Alloys, vol. 12, IFI/Plenum Press, New York, 1975.
[15] Personal communication to C. Lösch-Will, Ruhr-Universität Bochum, Materials Research Center, Bochum, Germany, 2002.
[16] M.O. McLinden, Meas. Sci. Technol. 17 (2006) 2597–2612.
[17] C.J. Smithells, Smithells Metals Reference Book, seventh ed., Butterworth–Heinemann, Boston, 1997.
[18] G.W. Burns, M.G. Scroger, G.F. Strouse, M.C. Croarkin, W.F. Guthrie, Temperature-electromotive force reference functions and tables for the letter-designated thermocouple types based on the ITS-90, National Institute of Standards and Technology, NIST Monograph 175, 1993.
[19] T.B. Coplen, J. Phys. Chem. Ref. Data 30 (2001) 701–712.
[20] R. Span, E.W. Lemmon, R.T. Jacobsen, W. Wagner, A. Yokozeki, J. Phys. Chem. Ref. Data 29 (2000) 1361–1433.
[21] W. Duschek, R. Kleinrahm, W. Wagner, M. Jaeschke, J. Chem. Thermodyn. 20 (1988) 1069–1077.
[22] M. Jaeschke, H.M. Hinze, Fortschr.-Ber. VDI, Reihe 3 262 (1991).
[23] J. Klimeck, R. Kleinrahm, W. Wagner, J. Chem. Thermodyn. 30 (1998) 1571–1588.
[24] A. Michels, H. Wouters, J. De Boer, Physica 1 (1934) 587–594.
[25] A. Michels, H. Wouters, J. De Boer, Physica 3 (1936) 585.
[26] P. Nowak, E. Kleinrahm, W. Wagner, J. Chem. Thermodyn. 29 (1997) 1137–1156.
[27] J. Otto, A. Michels, H. Wouters, Phys. Z. 35 (1934) 97.
[28] N. Pieperbeck, R. Kleinrahm, W. Wagner, J. Chem. Thermodyn. 23 (1991) 175–194.
[29] P.T. Boggs, R.H. Byrd, J.E. Rogers, R.B. Schnabel, User's reference guide for ODRPACK version 2.01 software for weighted orthogonal distance regression. National Institute of Standards and Technology, NISTIR 4834, 1992. The ODRPACK software is available at http://www.netlib.org/odrpack/.
[30] J.J. Hurly, M.R. Moldover, J. Res. NIST 105 (2000) 667–688.
[31] B.E. Gammon, J. Chem. Phys. 64 (1976) 2556–2568.
[32] A.L. Blancett, K.R. Hall, F.B. Canfield, Physica 47 (1970) 75–91.
[33] M.R. Moldover, J. Res. NIST 103 (1998) 167–175.
[34] L.A. Watts, Fluid Phase Equilibr. 217 (2004) 35–36.